OST Technical Progress Report
Innovative Technology Team -- FY2001 Results

Team Members: Duane H. Smith (Team Leader), Robert T. McLendon, Mara Dean, Martin Ferer, Goodarz Ahmadi, Kal Seshadri, S. Van Ooteghem, S. Beer, P. Yue, R. Pineault, Joseph W. Wilder, Wu Zhang, Amy Jones (WVU), Chung Ji (Clarkson University), H. O. Kono (WVU), F. Song (WVU), Robert P. Warzinski, Ronald J. Lynn, and Jerry J. Foster

Description: The Innovative Technology Team addresses potential means of enhancing energy production in an environmentally friendly manner. Research in FY01 focused on improved oil recovery, natural gas hydrates, and bacterial production of hydrogen.

For oil recovery, the team is developing new, critical-scaling equations of state for gases, liquids, supercritical fluids, and gas-liquid equilibria. The objective is to develop new equations to replace ubiquitously used cubic equations of state (such as Peng-Robinson), which have been known for several decades to have an incorrect mathematical form. Also, for oil recovery, the team is developing a network model for two-phase flow through porous media. This model is capable of treating both miscible and immiscible fluids, horizontal flow (no gravity/density effects), and vertical flow (in which density differences may be important).

For natural gas hydrates, the team is performing experiments and interpretations for the effects of pore size on hydrate equilibrium gas pressures and enthalpies of decomposition, experiments and modeling for production of natural gas from hydrates, and experiments and engineering computations for safety and stability concerns of seafloor hydrates. The objectives of the research described in this report are to obtain high quality scientific data and information that can be used for predictive modeling of the production of natural gas from gas hydrate deposits. This includes determining the phase behavior and thermal properties of hydrate samples obtained or prepared in porous media and relating these important properties to the composition of the samples.

The team is also conducting research on production of hydrogen from organic wastes using thermophilic bacteria.

RESEARCH OBJECTIVES: Research goals for FY01 for oil recovery included development and testing of scaling-theory equations for isotherms of single-component gas/liquid/supercritical fluid systems and completion of a computerized code for a network model of horizontal, immiscible, two-phase flow through porous media wetted by the displaced fluid.

For hydrates, the research goals included: (1) completion of equilibrium pressure-temperature measurements and data interpretations for sI and sII hydrates with a single-component guest in porous media of four different pore size distributions; (2) modification and calibration of experimental equipment to measure multi-component gas composition-pressure-temperature equilibria of hydrates in porous media; (3) writing and utilization of one-dimension numerical models for gas production and evaluation of other public-access codes for production of natural gas from hydrates by depressurization; (4) completion of initial-phase laboratory experiments on gas production from hydrates; (5) computer

simulations for safety and seafloor stability; (6) acquisition of equipment for measurement of triaxial strengths of hydrate-cemented sediments; and (7) making significant refinements to the experimental equipment and procedures used to obtain thermal property information on methane hydrate samples of known composition, both to improve the means for detecting the formation of hydrate in the high-pressure equipment and for the sensitivity of the thermal property measurements.

The overall goals for the bio-hydrogen project during FY01 were to develop a cost-effective continuous process for growing these organisms to produce maximal hydrogen concentrations. A key to doing this was achieving a better understanding of the biochemistry of the process.

LONG TERM GOALS / RELATIONSHIP TO NETL PRODUCT LINES: Both the phase studies and the flow studies address major, long-term problems encountered in reservoir simulations of oil recovery. The long-term goal of the phase behavior work is to develop more accurate, theoretically sound equations of state for fluids commonly encountered in secondary and tertiary oil recovery. The long term objective of the flow research is to determine the conditions under which (1) conventional fractional flow assumptions are correct, (2) fractional flow assumptions are incorrect, because the flow behavior is fractal, or (3) the flow behavior is in the transition or "crossover" region between fractional and fractal flow. Funds were received for this work from the National Petroleum Technology Office (NPTO) in Tulsa, OK.

The FY01 hydrates tasks supported the long term characterization, production, and safety and seafloor stability goals of the national natural gas hydrates program, as described in the DOE program plan. Funds were received from the Gas Exploration, Production, and Storage product line, which is a component of NETL's Strategic Center for Natural Gas.

The goal of the bio-hydrogen research is to develop a cost-effective method to convert organic materials, ideally organic wastes, into hydrogen fuel, through the activity of biological processes. Funds for the bio-hydrogen research came from the NETL Advanced Research Product Line and DOE's Office of Energy Efficiency and Renewal Energy.

FY 2001 RESULTS

SECONDARY AND TERTIARY OIL RECOVERY--PHASE STUDIES AND PORE-LEVEL MODELING

Injection of fluids into oil reservoirs is a commercially proven method of secondary and tertiary oil recovery. However, it has long been known that in these processes, displacement of the oil by the less-viscous fluids causes unstable displacement fronts, which permit only a fraction of the oil to be recovered. A better understanding of the fluid displacement process could lead to reduced capital and operating costs for this technology.

We have approached this problem from three complementary fronts: i) reduction in sweep efficiency due to viscous fingering in miscible flooding of oil reservoirs by carbon dioxide, ii) reduction in sweep efficiency because of capillary blocking during immiscible floods, and iii) phase coexistence of the oils and the injected fluids. We had developed a pore-level model of miscible injection where a less viscous

fluid (e.g., carbon dioxide) is used to displace a more viscous fluid (e.g., oil). Recently, we have developed a pore-level model of the immiscible injection of a non-wetting fluid into a porous medium saturated with a wetting fluid to model the displacement of oil in oil-wet reservoirs. As a first-step in reliably modeling complicated phase equilibrium, we have used correct critical scaling relations with appropriate modifications to provide a predictive model of the supercritical isotherms of simple fluids.

The computer code for the pore-level models satisfies fluid conservation to within a fraction of a percent. The model of miscible flooding incorporates only the fluid viscosities. The model of immiscible flooding is a modification of the earlier miscible model; this version incorporates the fluid viscosities and the interfacial tension between the fluids, as well as gravitational over-ride effects. In this immiscible model, the pressure drop across any one of the throats in the medium must overcome both viscous, capillary, and gravitational forces to move the fluids through the pore throats of the medium. The computer code maintains a constant injection velocity to within a few percent, which is essential in maintaining a constant capillary number.

Our pore-level model is intended to incorporate, as realistically as possible, both the capillary pressure that tends to block the invasion of narrow throats and the viscous pressure drop in a flowing fluid. The two-dimensional porous medium was modeled as a diamond lattice (see below), which consists of pore-bodies of volume, ℓ^3, at the lattice sites; connecting these pore-bodies are throats which are of length, ℓ , and have a randomly chosen cross-sectional area between 0 and ℓ^2.

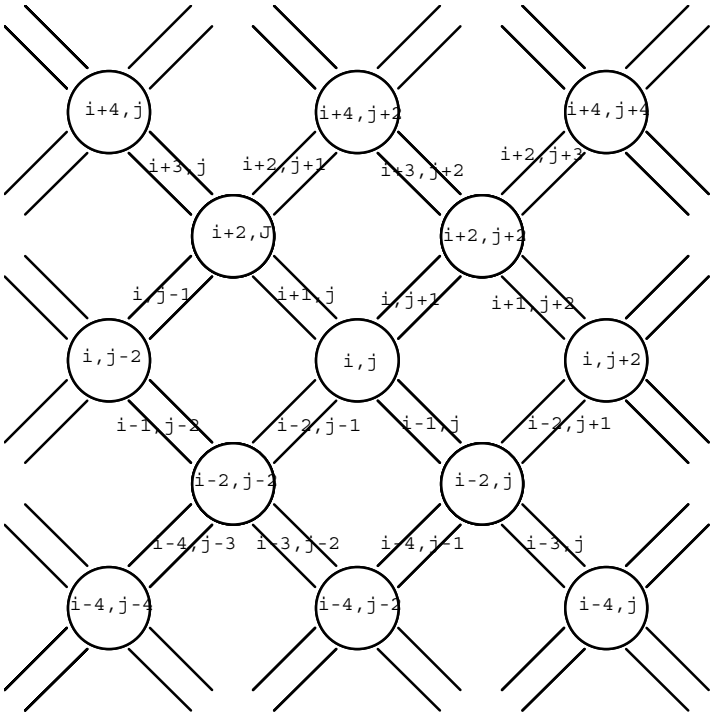

Figure I.1. A portion of the two-dimensional porous medium.
The pore bodies, labeled by two even integers, occupy the sites of a diamond lattice. Adjacent pore bodies are connected by pore throats, which are labeled, as shown, by one even and one odd integer. The diamond lattice structure was chosen instead of a square lattice to minimize spurious blocking of throats

that are perpendicular to the direction of average flow.

Our model should be both more general and more flexible than several models reported in the recent literature, in part because both the throats and the pore-bodies have finite volume. The other models assume either that the throats contain zero volume of fluid or that the pore-bodies have zero volume. Furthermore, in our model, the volumes of both the pore-bodies and throats can be set as desired.
We found that the time interval through which the interface was advanced had to be chosen with care. Of course, if the interval is too small, the computer program will be unnecessarily inefficient. However, if the interval is too great, large, spurious oscillations occur in the fluid flow about the true equilibrium. For example, in throat A, (see Fig. I.2) too large a time step would cause the fluid to advance too far (to a region with too large a capillary pressure for the pressure drop); at the same time, the fluid in throat B would retreat too far (to a region with too small a capillary pressure for the pressure drop). Therefore, a strong restoring force would be set up; the large capillary pressure in A would push the fluid too far back, while the small capillary pressure in B would pull the fluid too far into the throat.

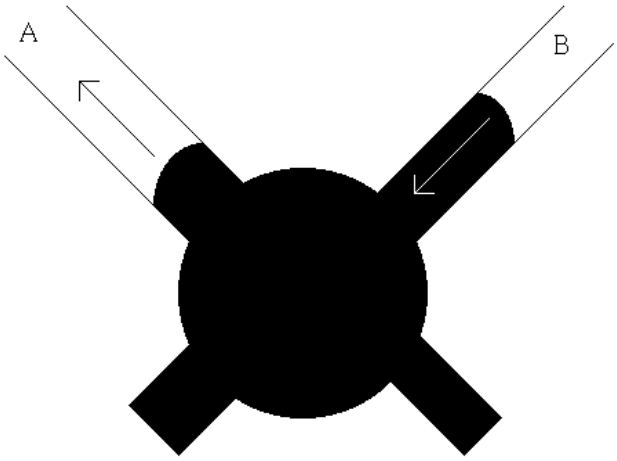

Figure I.2. If the time step is too big, the meniscus will advance too far into throat A to a region where the capillary pressure is significantly larger than the pressure drop so that in the next time step there is a large force in the opposite direction on this meniscus. When the meniscus in B moves too far towards the inlet, the capillary pressure decreases too much so that there is a large force in the opposite direction on the meniscus in B.

Implicit in this discussion is the assumption that the pressure within a pore-body is uniform. Assuming otherwise would require doing full fluid dynamics using the Navier-Stokes equations. This is inconsistent with the pore-level model approach and, given finite computer resources, this would severely limit the size of the model porous medium.

Once the pressure field has been determined, the interface can be advanced through a time interval Δt. A throat is considered to be on the interface if the pore-body at one end contains some wetting fluid (it may be filled with wetting fluid) and if the pore-body at the other end is fully invaded by non-wetting fluid (or was fully invaded and is not yet fully re-invaded by wetting fluid due to backflow). As discussed earlier, a time interval Δt, needs to be chosen which is small enough that spurious local oscillations in the flow are avoided, but not so small that the program run-time is unnecessarily long. For the cases

discussed here with large surface tension, the following prescription seems adequate. For all interfacial throats where the non-wetting fluid has yet to reach the midpoint of that throat (meaning that the capillary pressure is still increasing), the time interval is chosen so that the non-wetting fluid advances no more than 3.5% of the total length into any such throat. For all interfacial throats where the non-wetting fluid has advanced past the midpoint (meaning that the capillary pressure is decreasing), the time step allows the interface to advance no further than 33% of the total length into any such throat. Having determined the interface and chosen the time step, we have attempted to make the flow rules as non-restrictive and reliable as possible:

i) All elements of the porous medium (pore-throats and pore-bodies) have volumes that can be occupied by either type of fluid.

ii) Locally, back-flow as well as forward-flow is allowed, as ordained by the local pressure differences.

iii) Complications, such as over-filled pore-bodies or plugs of fluid trapped in the pore throats, are treated as physically as possible.

iv) Unphysical aspects, such as isolated 'blobs' of wetting fluids residing in pore-bodies, are tracked by the program and found to be of insignificant magnitude.

v) Most importantly, the flow rules accurately account for all of the non-wetting fluid injected into the porous medium. For the smallest capillary number, there is a 0.25% difference between the volume of non-wetting fluid injected into the medium and the volume of non-wetting fluid occupying the medium as determined by the flow rules. For the largest capillary number, this difference is less than 0.01%.

At present, our computer code models the flow in two-dimensional porous media. It should be straightforward to modify our code so that it models flow in three-dimensional porous media; however, computer time considerations will limit this modeling to systems of smaller lateral size than the two-dimensional systems presently under consideration.

The model described above reproduces the results of the earlier miscible flooding model when the interfacial tension is set equal to zero. In summary, this work showed detailed results illustrating that the flows began as diffusion-limited aggregated fractals, which produces very sparse fingering with a saturation profile decreasing almost exponentially from inlet to outlet, resulting in minimal sweep efficiency. However, in all cases, the flow became compact at a time that decreases as the viscosity of the injected fluid is increased. Therefore, all real injected fluids eventually form a stable saturation front advancing through the medium. Our determination of the fractal-to-compact crossover enabled a prediction of the dependence of fractional flow upon viscosity and saturation.

Because the role of capillary forces must be understood before one can study the intriguing problems involved with combining viscous with capillary effects, we fixed the viscosity ratio at the value of unity. Both injected and displaced fluids have the same viscosity, so viscous effects cannot affect fingering. Therefore, any effects will be due solely to the role of capillary forces. At sufficiently low capillary numbers, our model correctly reproduces the zero-capillary number results from invasion percolation with trapping (IPwt).

Most of the results from the flow model are from systems that are either 30x90 or 30x135. Because invasion percolation is such a noisy process, it proved difficult to study the change from invasion percolation to more piston-like flow. To show the effect of the noise and how the change occurs, we present graphs that compare results for invasion percolation (solid line) with those from the model (dashed line) for two capillary numbers for the quantity $\langle x \rangle / (0.445\, t^{1.13})$. In all cases, the results from the model begin by following the invasion percolation results quite closely but then deviates at a later time, which decreases as capillary number increases.

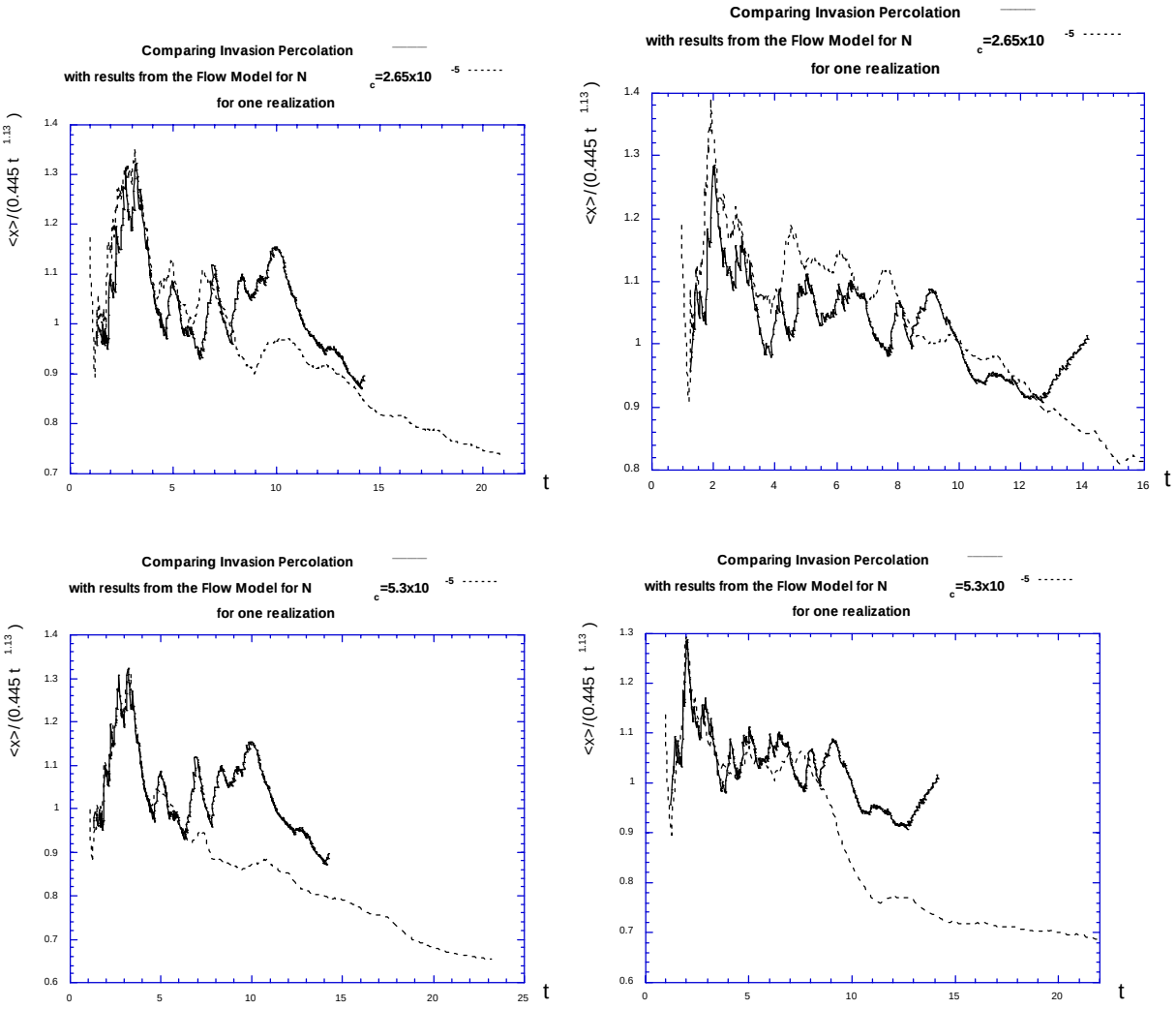

Figure I.3. Comparison of flow model results (dashed lines) for 2 capillary numbers ($N_c=2.65\text{x}10^{-5}$ in the top figures and $N_c=5.3\text{x}10^{-5}$ in the bottom figures) with results from IPwt (solid lines) for realizations #1 (left hand figures) and #2 (right hand figures). Note that the solid curves are the same for both figures for realization #1 (also for both figures for realization #2).

To estimate the dependence of the characteristic time upon capillary number, we have attempted to collapse all of the data onto one curve. The form of characteristic time that most effectively accomplishes this collapse is

$$\tau(N_c) = \{ \ln (1 / N_c) \}^{2.5} , \qquad (1)$$

where our crude estimate of the uncertainty in the exponent is 2.5 ± 0.5 in that 2.0 is too weak a dependence and 3.0 is too strong a dependence. This form for the characteristic time provides a credible collapse of the data so that

$$\langle x(t) \rangle = 0.445\, t^{1.13}\, F(t/\tau)\ . \qquad (2)$$

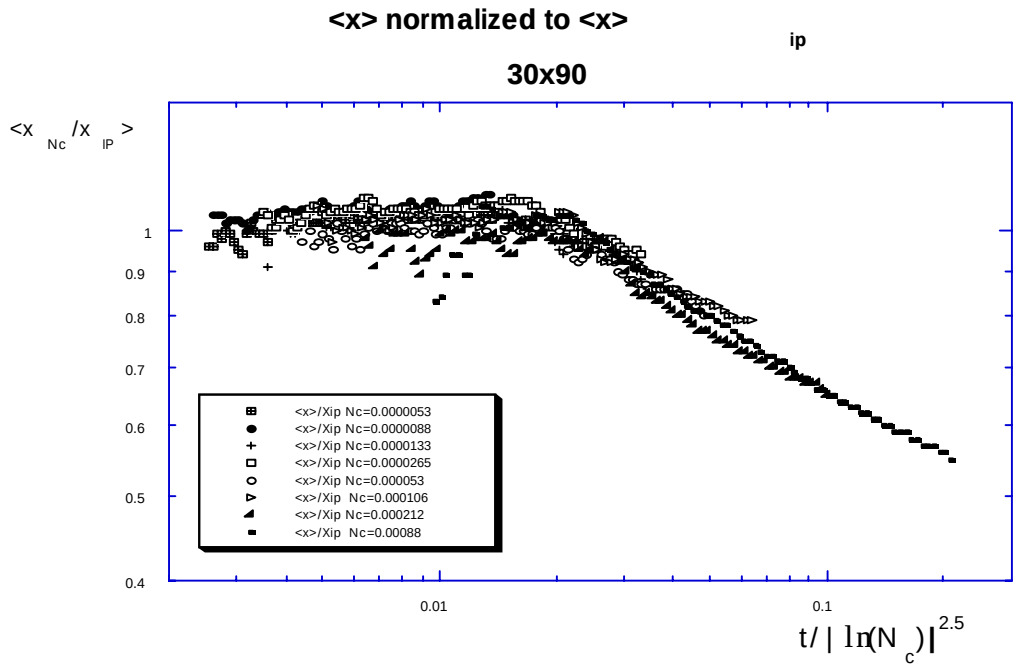

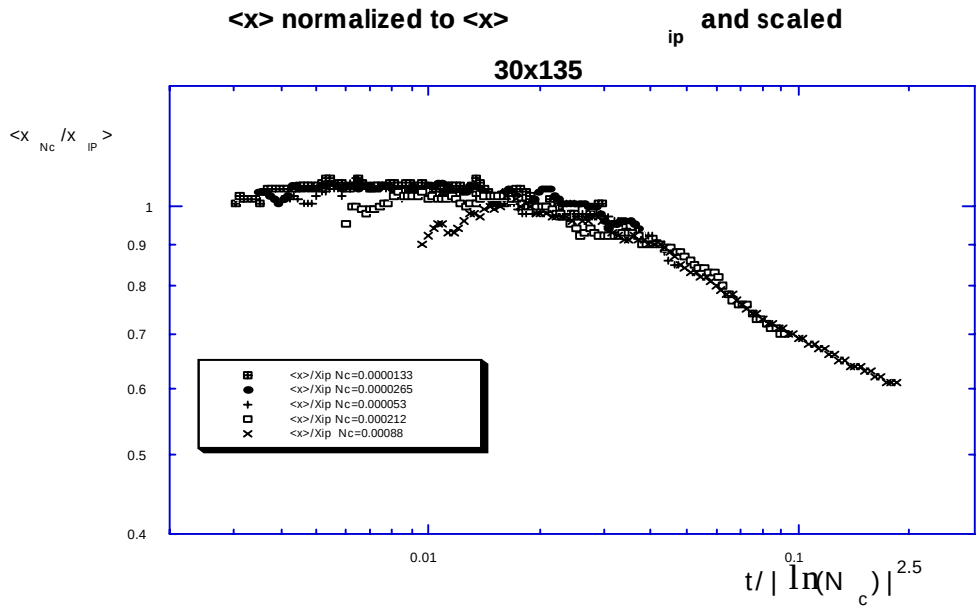

Figures I.4 and I.5 show the collapse of the data using the characteristic time.

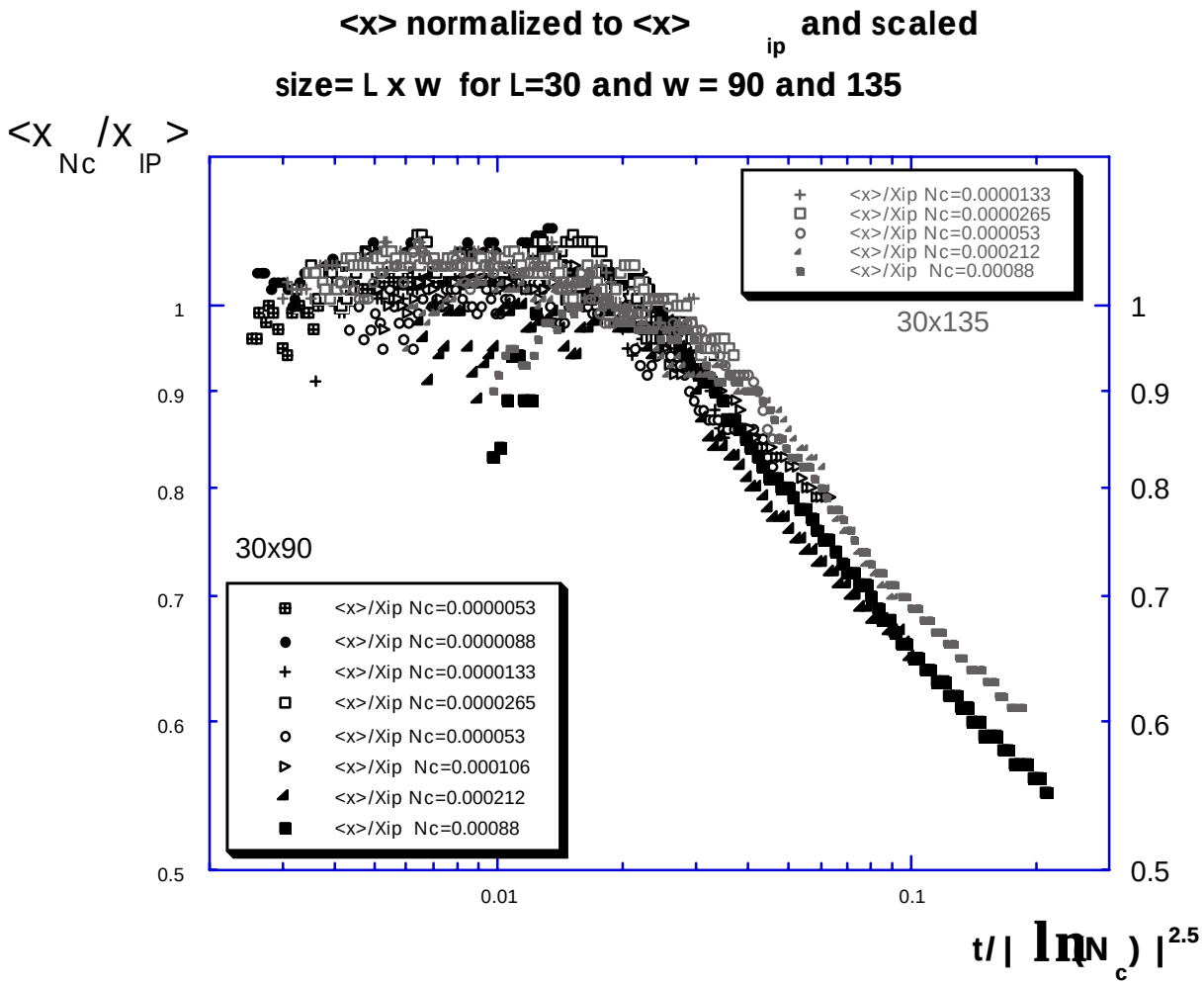

Figure I.6 combines the data from Figures I.4 and I.5.

We ran our computer code on systems that were 90 pores wide by 30 long (in the direction of average flow) using typical experimental values for surface tension and viscosity. We chose to model our flow on short and wide systems, since long and narrow geometries are known to misrepresent the fingering because of coarsening. Figure I.7 shows some typical, near-breakthrough fingering patterns where the non-wetting fluid is injected along the lower edge.

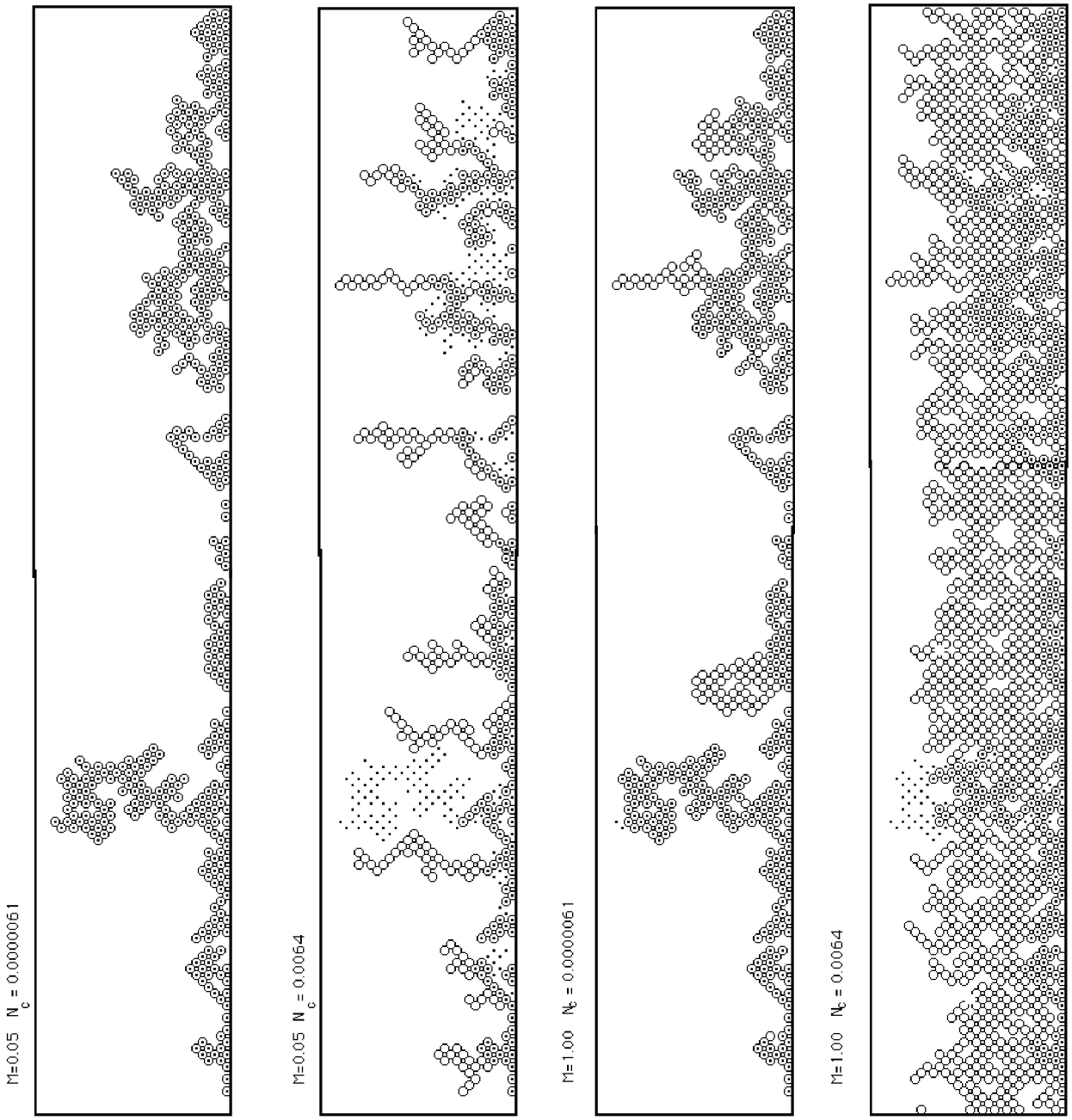

Figure I.7 shows the occupation of a particular realization of a model porous medium. The small solid circles show the CO_2 occupation as predicted by IPwt. The open circles show the CO_2 occupation as predicted by our pore-level model for M=0.05 and M=1 at two different Capillary numbers.

Figure I.8 shows near-breakthrough saturation profiles for a wide range of capillary numbers with viscosity ratio M=0.05. The data points show averages over 5 different realizations of the porous medium (i.e., for each realization, a different seed was used in the random number generator to determine the cross-sectional area of each throat); the error bars show the standard errors from the set of five realizations. Over this wide-range of capillary numbers, there is little difference between the saturation profiles or between the total breakthrough saturations of injected fluid, which are all around 20% or less.

Although the effect of capillary number on non-wetting-fluid saturation is small, if not negligible, capillary number has a significant effect upon the geometry of the fingering. For M=0.05, Figure I.8a shows that the fingering for a low capillary number, $N_C = 6.25 \times 10^{-6}$, is identical to the fingering for IPwt. Using the same model porous medium, the non-wetting occupation from our model for this low capillary number is shown by the open circles, while the non-wetting occupation from the IPwt is given by the small filled circles. That is, when the pore body location is marked by an open circle with a small filled circle inside, that same pore body was occupied by non-wetting fluid using our model and independently by non-wetting-fluid using IPwt. For the five model porous media on which we've run the model, the agreement between IPwt and the model was excellent. In the worst case, the occupation of seven pore bodies was different between our model and IPwt. For the model porous medium shown in Figure I.8, the non-wetting occupation from the model and IPwt are identical. Figure I.8b shows the non-wetting occupation at a larger capillary number for this same porous medium. Of course, since this is the same porous medium as that shown in Fig. (I.8a), the IPwt occupation, shown by the small filled circles, is the same for both. However, the fingering from the model at this large capillary number is very different from the IPwt fingering in Fig.I.8a. Indeed, at large capillary number the fingering from the model (open circles) is visually similar to DLA fingering.

These low saturations for M=0.05 are to be contrasted with the saturations that can be achieved at larger viscosity ratios. For the same capillary numbers (i.e. the same surface tension and volume flows), we have performed the simulations with viscosity ratio, M=1. The results are very different. At small capillary number, the M=1 saturations and fingering are identical to Ipwt, as they should be. However, as capillary number increases, the flows become compact with negligible fingering and the saturations increase dramatically The breakthrough saturations are nearly constant for M=0.05, whereas they increase significantly for the larger viscosity ratio M=1.0.

Our results from simulations show that injection of low viscosity non-wetting fluid into the two-dimensional porous medium leads to small fractional saturations at breakthrough yielding a small sweep efficiency. If the viscosity of the injected fluid could be increased, these results suggest that the sweep efficiency could be doubled. Since this work has been done on small systems with only two viscosity ratios, it is important to ascertain how these effects change when one scales-up to realistically-sized systems. It is also important to determine how this effect depends upon the viscosity ratio throughout the range of physical interest.

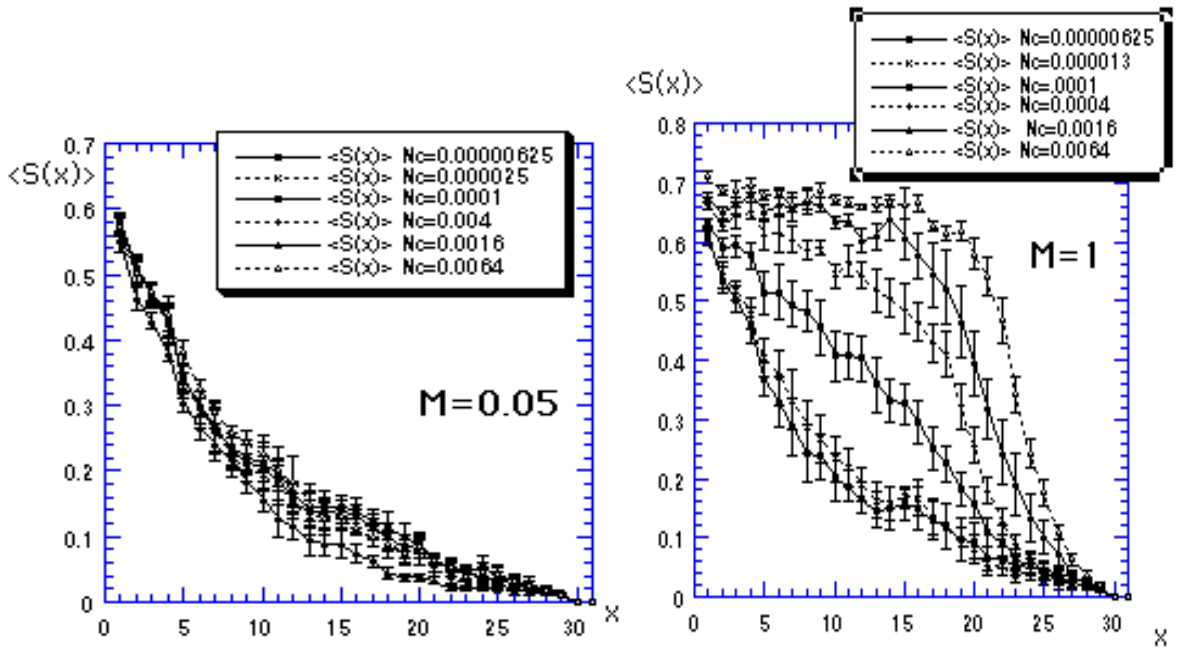

Figure I.8 shows the near-breakthrough saturations for viscosity ratios M=0.05 (left-hand figure) and M=1.00 (right hand figure) for a range of capillary numbers from 6.25×10^{-6} to 6.4×10^{-3}.

For CO_2, [12] the critical temperature and critical pressure are well characterized by experiment and the values T_C = 304.21K, V_C = 94.09 $\frac{cm^3}{mole}$, and P_C = 73.83 bar. For ethane, T_C = 305.56, V_C = 149.9$\frac{cm^3}{mole}$, and P_C = 4.89MPa; [13],[14], [15] and for methane, T_C = 190.52K, V_C = 97.69 $\frac{cm^3}{mole}$, and P_C = 4.60 MPa. [16]

The extended critical equation of state requires input from fitting three measured quantities: a) the phase boundary or coexistence curve, b) the critical isotherm, and c) the temperature dependence of the vapor pressure and critical isochore.

The function used in fitting the critical isotherm is modified to include three temperature-dependent fitting parameters and is then used to fit the supercritical isotherms. Critical scaling predicts temperature dependencies for these three fitting parameters. Having determined the temperature-dependence of these three fitting parameters, we have a predictive model for generating any supercritical isotherm that is accurate for all pressures and for all temperatures above the critical temperature.

We have previously demonstrated the advantages of using a modified order-parameter (OP) (modified molar volume - MMVc)

$$OP = MMV - MMV_C = T \ln\left(\frac{V-b}{aT}\right) - Tc \ln\left(\frac{V_c-b}{aT_c}\right)$$

where V is the molar volume, T is the temperature, and a is chosen to make the argument of the logarithm dimensionless (e.g., a = 1 $\frac{cm^3}{mole\ K}$). This form incorporates a Van der Waals excluded volume, b, and the logarithmic form dictated by the known behavior of the vapor pressure in the ideal gas limit. The values used in this report are b = 29.9 $\frac{cm^3}{mole}$ for carbon dioxide, b = 20 $\frac{cm^3}{mole}$ for ethane, and b = 27.5 $\frac{cm^3}{mole}$ for methane; the fits do not seem particularly sensitive to precise values of this fitting parameter. The previous publication demonstrated the efficacy of this form of the order parameter for carbon dioxide, several alkanes, and a refrigerant.

<u>Carbon Dioxide</u>

$(OP_V - OP_L)/2 = m1(1-T/304.21)^{0.325}(1+m2(1-T/304.21)^{0.55})$

$OP= T\ Ln((V-29.9)/T)$

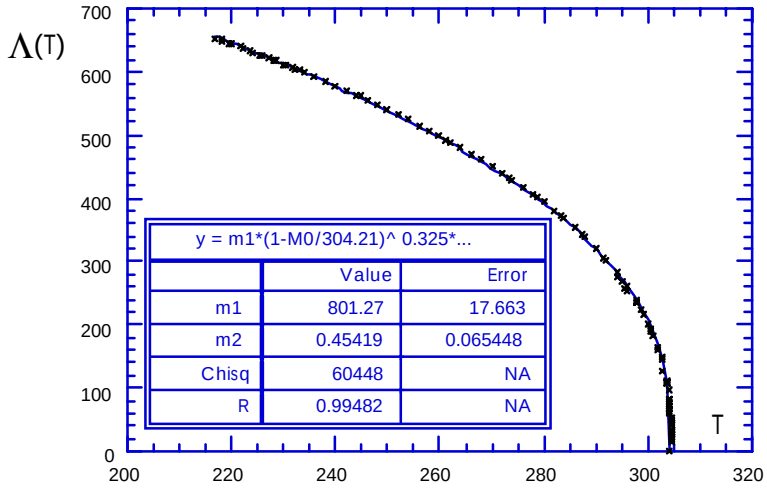

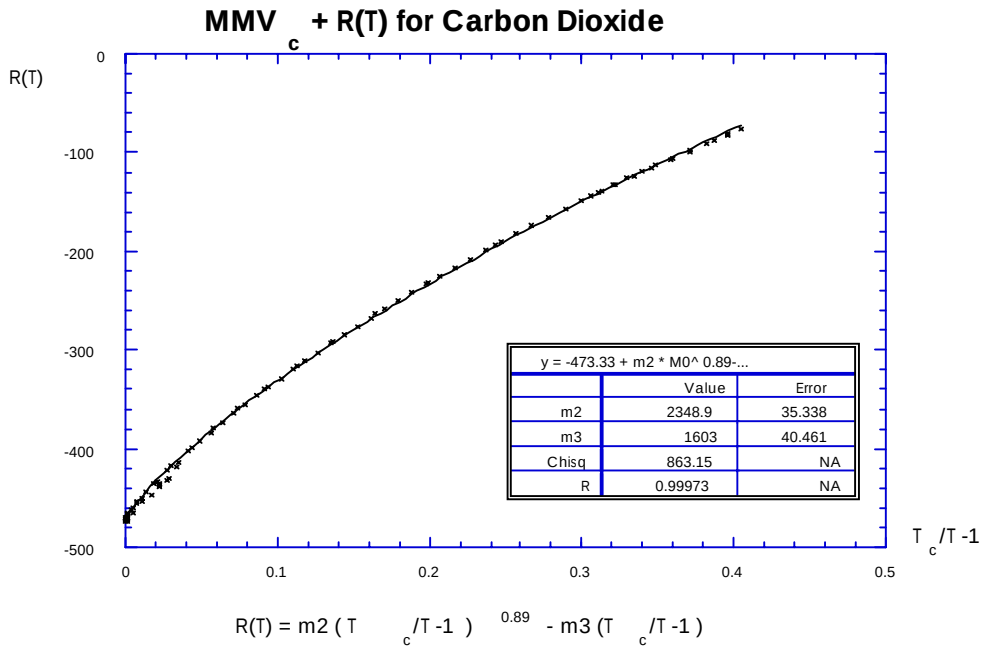
MMV c + R(T) for Carbon Dioxide
R(T)
0
-100
-200
-300
-400
-500
0
0.1
0.2
0.3
0.4
0.5
T c /T -1
y = -473.33 + m2 * M0^ 0.89-...
Value
Error
m2
2348.9
35.338
m3
1603
40.461
Chisq
863.15
NA
R
0.99973
NA
R(T) = m2 (T c /T -1) 0.89 - m3 (T c /T -1)

Ethane

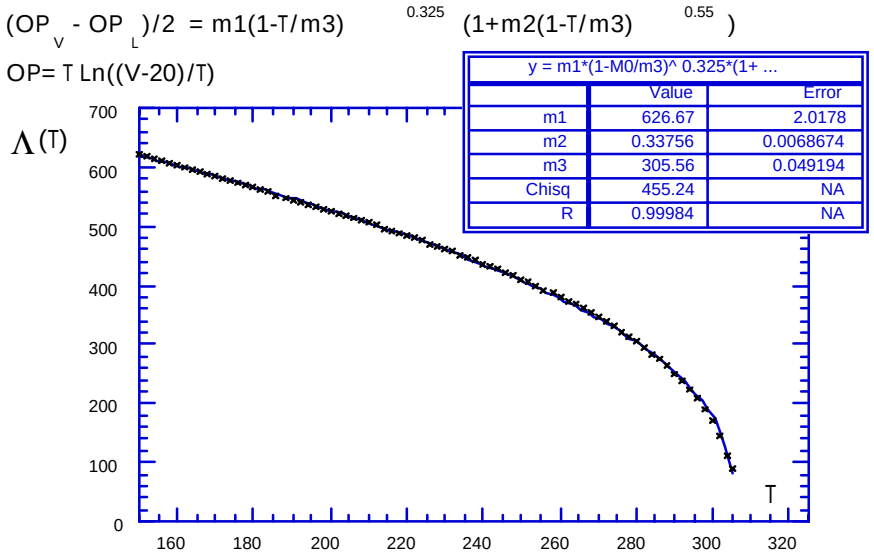
(OP V - OP L)/2 = m1(1-T/m3) 0.325 (1+m2(1-T/m3) 0.55)
OP= T Ln((V-20)/T)
Λ(T)
700
600
500
400
300
200
100
0
160
180
200
220
240
260
280
300
320
T
y = m1*(1-M0/m3)^ 0.325*(1+ ...
Value
Error
m1
626.67
2.0178
m2
0.33756
0.0068674
m3
305.56
0.049194
Chisq
455.24
NA
R
0.99984
NA

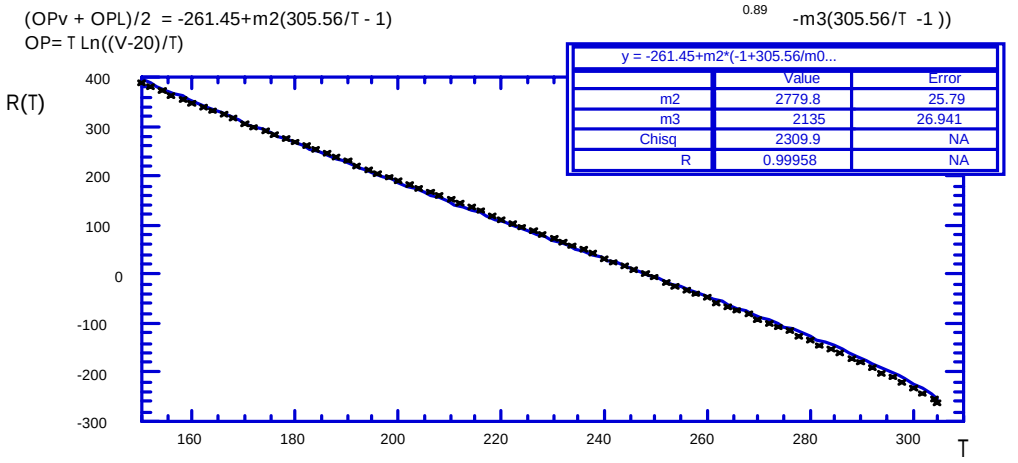

Methane

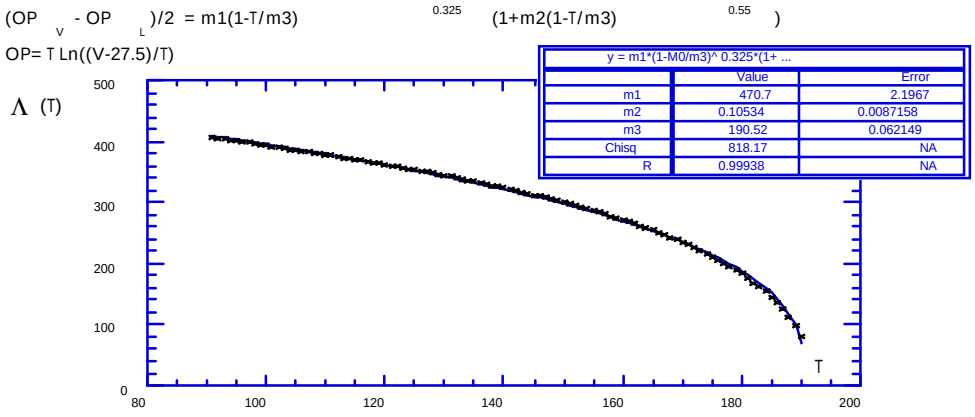

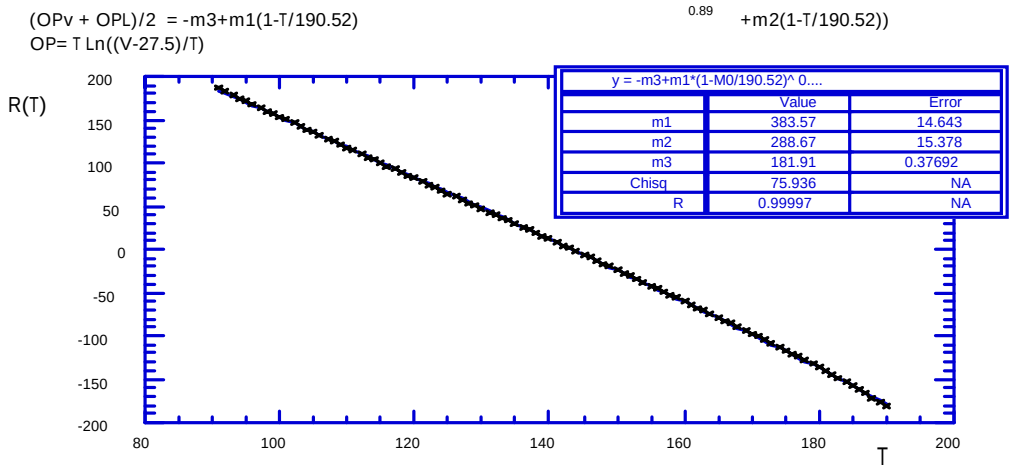

Fits of our equation of state, values of non-universal fitting parameters, and statistical measures of the goodness of fit for carbon dioxide, ethane, and methane.

For carbon dioxide, the fits determined values for the constants s = -184.9 ± 4.0, a = -0.04566 ± 0.006, and a value of the critical volume $V_c = 94.09 \pm 0.10 \frac{cm^3}{mole}$ consistent with the value from fitting the phase boundary. The dominant terms are the constant and the dependence linear in ΔP, which are designed to give the correct behavior in the ideal gas limit where

$$MMVIG = T_c \ln(\frac{V-b}{V_c-b}) = \sigma_2(\Delta P) - \sigma_2(\Delta P) = + T_c \ln(\frac{n R T_c}{(V_c -b)P_c}) - T_c \Delta P$$

so that rewriting ΔP

$$T_c \ln(\frac{V-b}{V_c-b}) = + T_c \ln(\frac{n R T_c}{(V_c -b)P_c}) - T_c \ln(P / P_c)$$

dividing through by the critical temperature throughout, combining all terms on the left-hand side, and using $V-b \approx V$ in the small P limit, one has

$$\ln(\frac{P V}{n R T}) = 0 \text{ or } \frac{P V}{n R T} = 1 .$$

On the high-pressure liquid side, the figure shows a nearly straight line with slope different from the slope on the small pressure side

$$MMV = \sigma_2(\Delta P) + \frac{1 - c}{1 + c} \quad \sigma_2(\Delta P) = - a_o + a_1 \Delta P - a_2 \ln(1 + a e^{\Delta P})$$

specifically, $MMV = MMVh(P>>1, T_c)$

$$OPh(P,Tc) = - \frac{1 - c}{1 + c} T_c \ln(\frac{n R T_c}{(V_c -b)P_c}) - (\frac{1 - c}{1 + c} T_c + \frac{2s}{1+c}) \Delta P + \frac{2f}{1+c} \ln(\frac{1+a}{1+ae^{\Delta P}})$$

The deviations from linearity in the large pressure regime is obviously well mimicked by the last term, which was suggested by the Van der Waals correction a/V^2, which gives corrections of order P^2 to the leading term P/nRT for the quantity 1/(V-b). In any case, the correction is small and other similar functions of $e^{\Delta P}$ provide equally good fits.

For temperatures below the critical point, the carbon dioxide data are from the IUPAC tables. For temperatures above the critical point, the data were estimated by extrapolating the isotherms to find the value of the pressure at the critical volume, Vc. The Clausius-Clapeyron equation predicts that the log of the pressure should go as A + B/T . Critical phenomena predicts that there should also be a dependence upon $|T - T_c|^{1-\alpha}$. We found excellent fits to the data using the functional form:

$$\ln(P(T)) = A + \frac{B}{T} + C (1 - \frac{T_c}{T})^2 + D (1 - \frac{T_c}{T})^{2 -\alpha} + \frac{E}{T^3}$$

These fits provide the critical isochore, determining how much the pressure deviates from that value giving the critical volume. Therefore, away from the critical temperature ΔP= ln(P/P(T)).

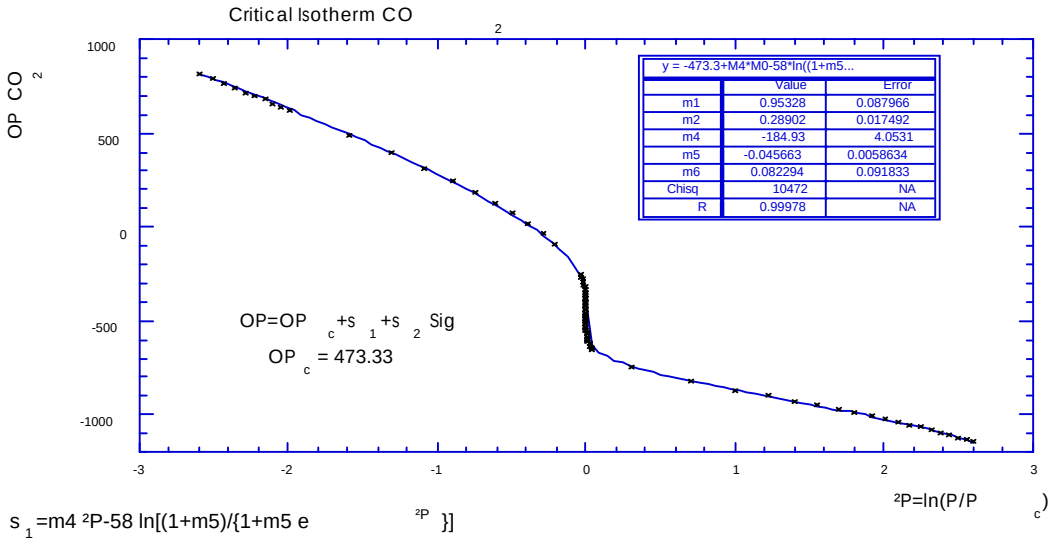

s_1 =m4 ²P-58 ln[(1+m5)/{1+m5 e ^{²P} }]

s_2 ={-473.33-36.095+(304.21+m4)²P-58 ln[(1+m5)/(1+m5 exp ^{²P})]}

Sig=(1-m2)/({ [abs(tanh [p])] $^{0.7917}$) /tanh[p] } + m2)

p=m1 ²P/(1+m6 ²P $^{0.72}$)

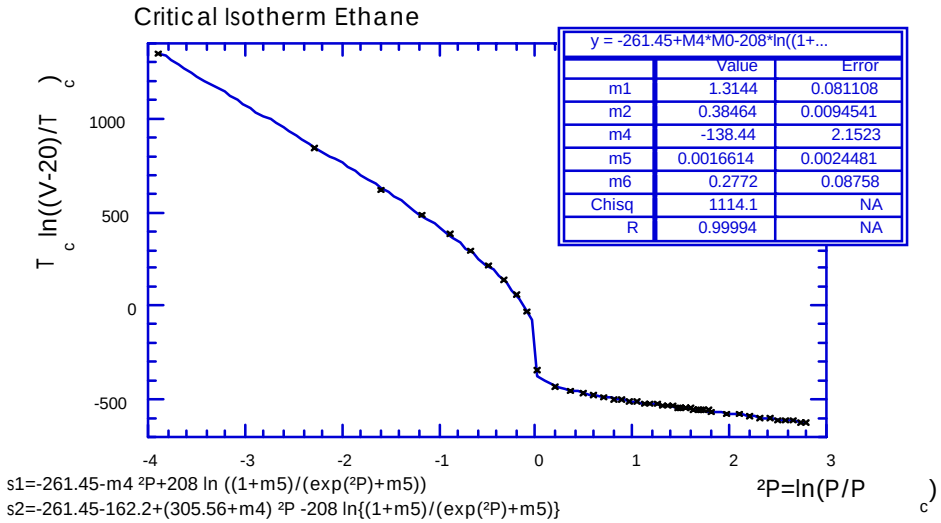

s1=-261.45-m4 ²P+208 ln ((1+m5)/(exp(²P)+m5))

s2=-261.45-162.2+(305.56+m4) ²P -208 ln{(1+m5)/(exp(²P)+m5)}

Sig=(1-m2)/{ [(abs(tanh (p)))^ 0.7917 /(tanh(p))]+ m2 }

p=m1²P/(1+m6 ²P^0.72)

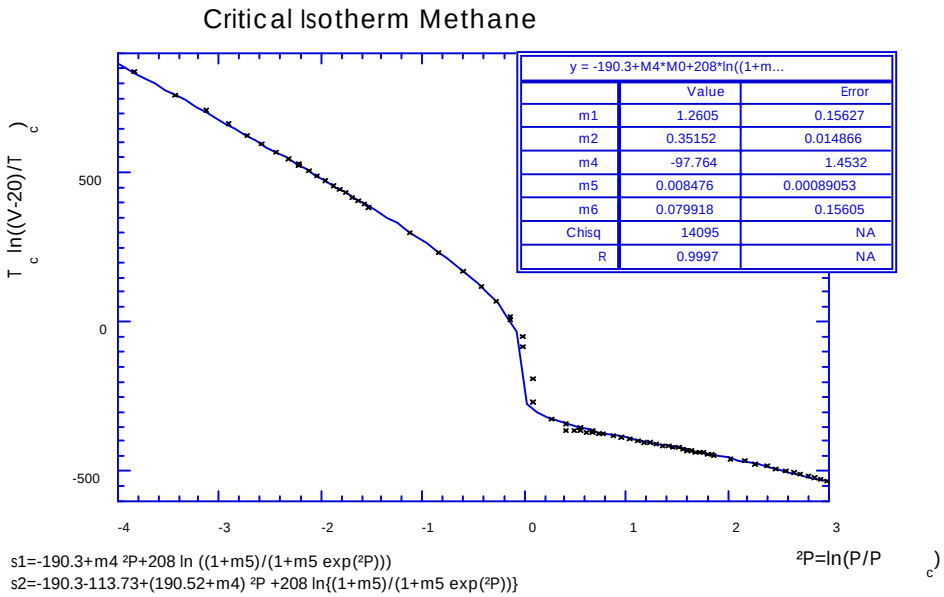

Data and fits for critical isotherms of carbon dioxide, ethane, and methane.

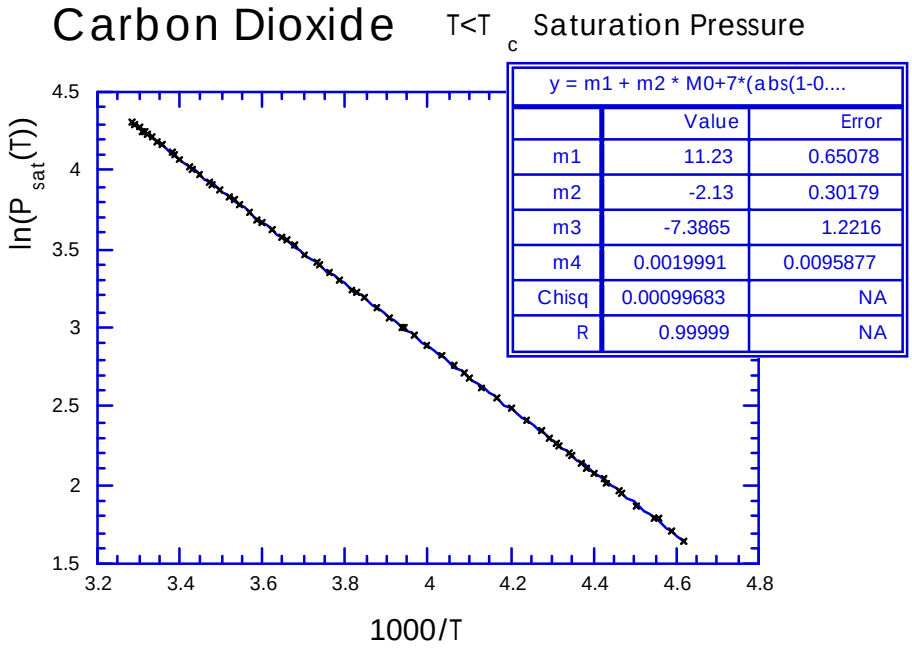

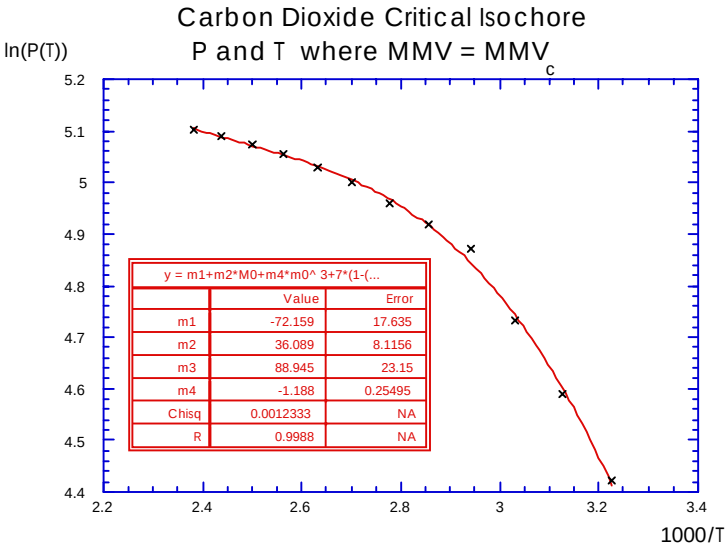

$$\ln(P(T)) = m1 + m2(1000/T) + m4\,(1000/T)^{3} + 7\,|\,1 - Tc/T\,|^{1.89} + m3\,|\,1 - Tc/T\,|^{2}$$

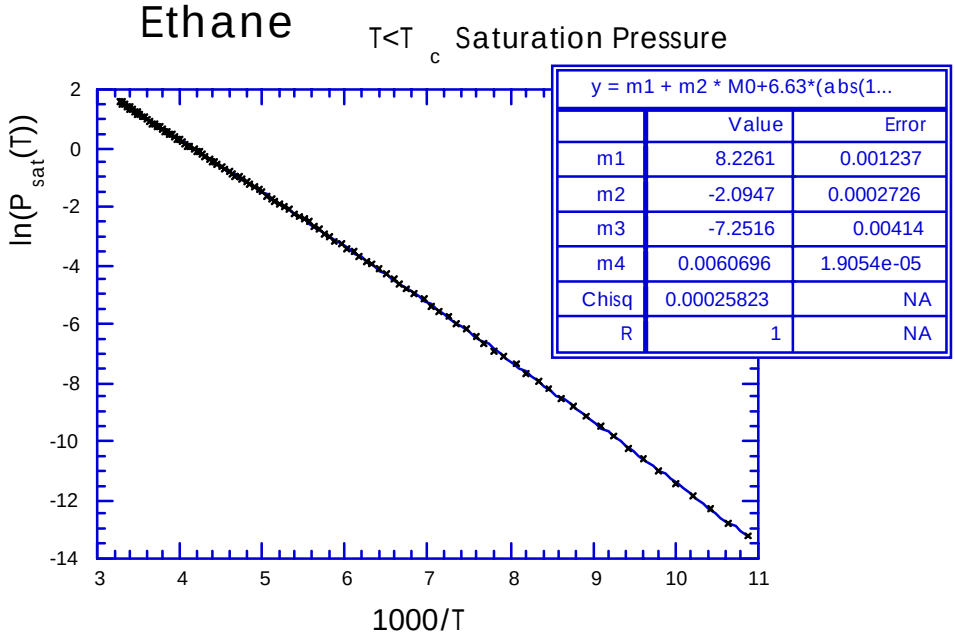

Ethane Critical Isochore
P and T where MMV = MMV$_c$

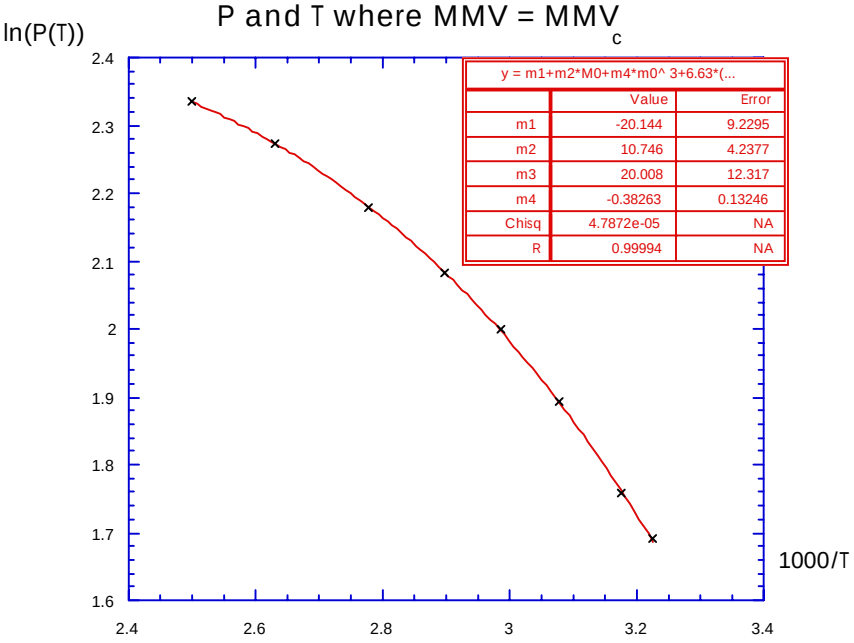

$$\ln(P(T)) = m1 + m2(1000/T) + m4\,(1000/T)^{3} + 6.63\,|\,1 - Tc/T\,|^{1.89} + m3\,|\,1 - Tc/T\,|^{2}$$

Methane $T<T_c$ Saturation Pressure

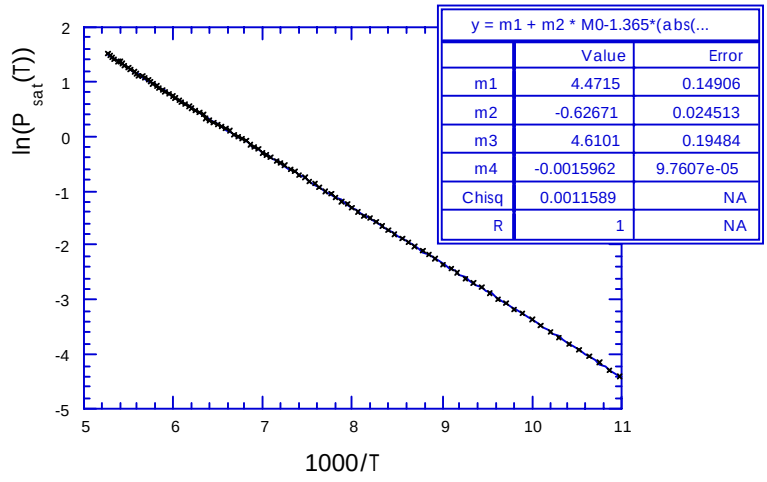

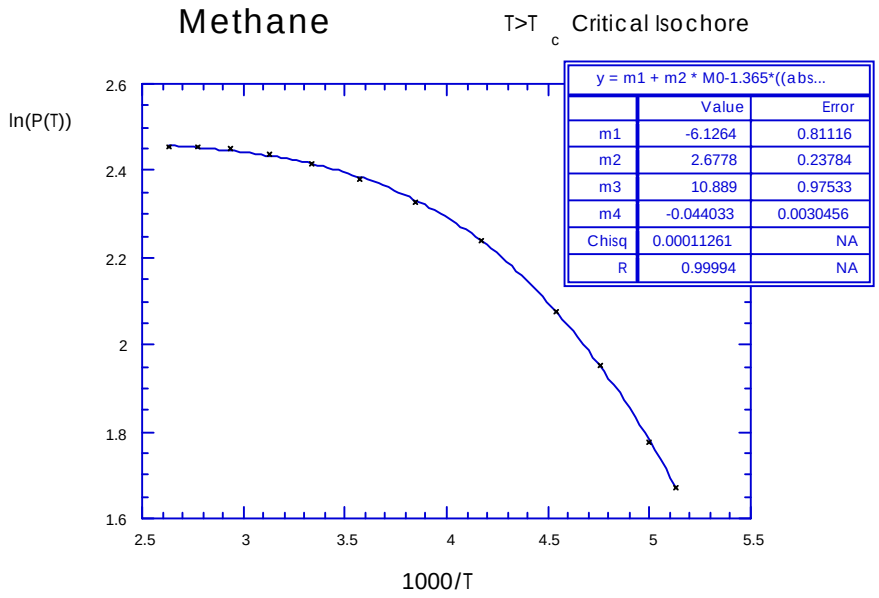

Saturation pressures and critical isochores for carbon dioxide, ethane, and methane.

Appropriate modifications of the function used to fit the critical isotherm can be used to predict the supercritical isotherms. The following graphs show these fitting parameters for the various gases with reasonable functional fits to each of the parameters:

Carbon Dioxide

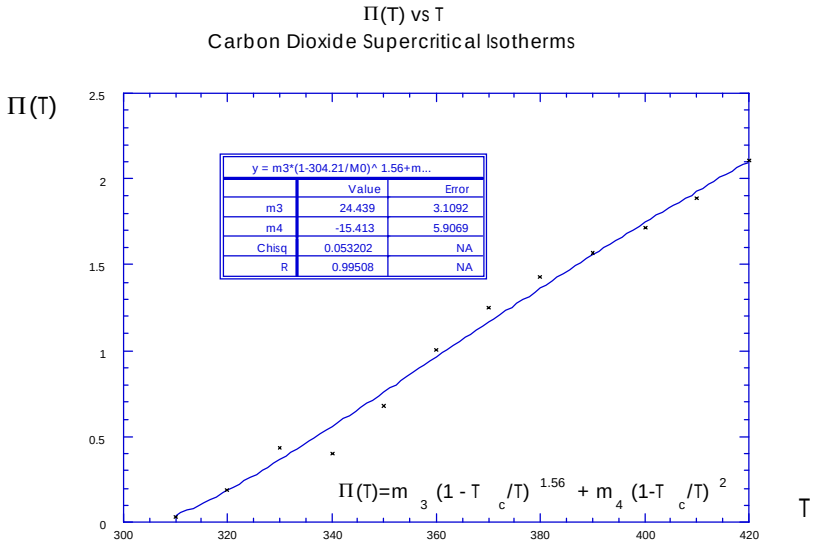

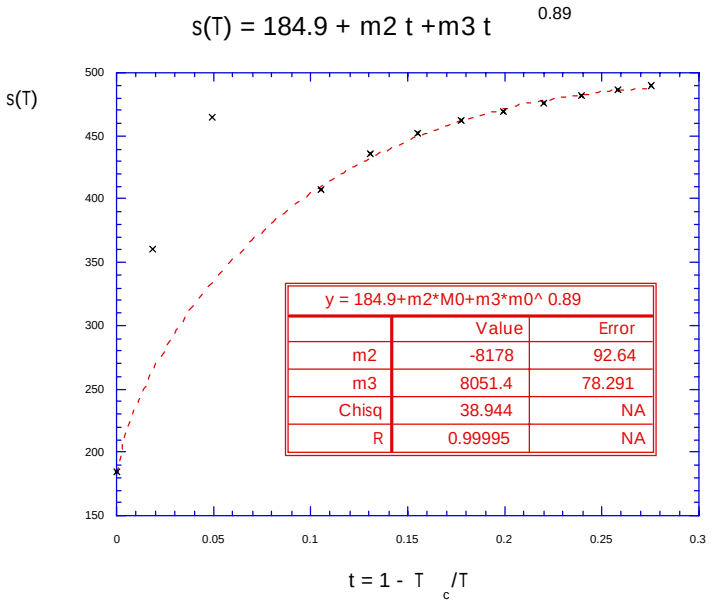

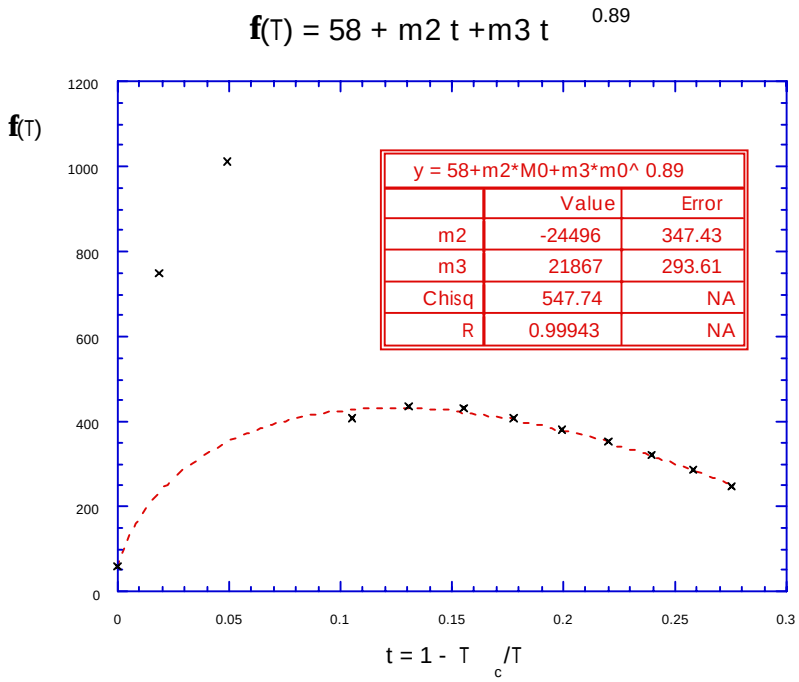

Plots of Π, s, and f for carbon dioxide.

Ethane

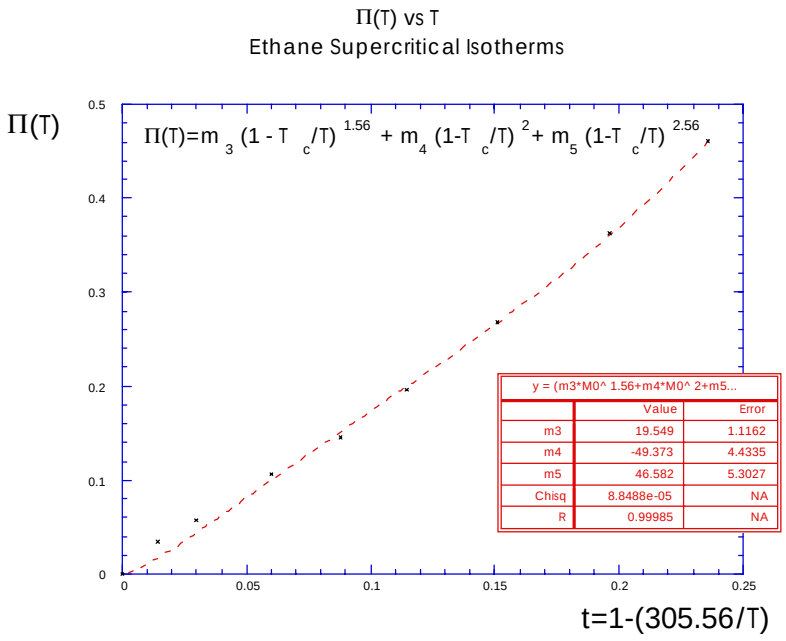

$$\mathbf{f}(T) = -m1+\{(208+m1) + m2\ t + m3\ t^{0.89}\}/\{1+ m4\ t^{3}\}$$

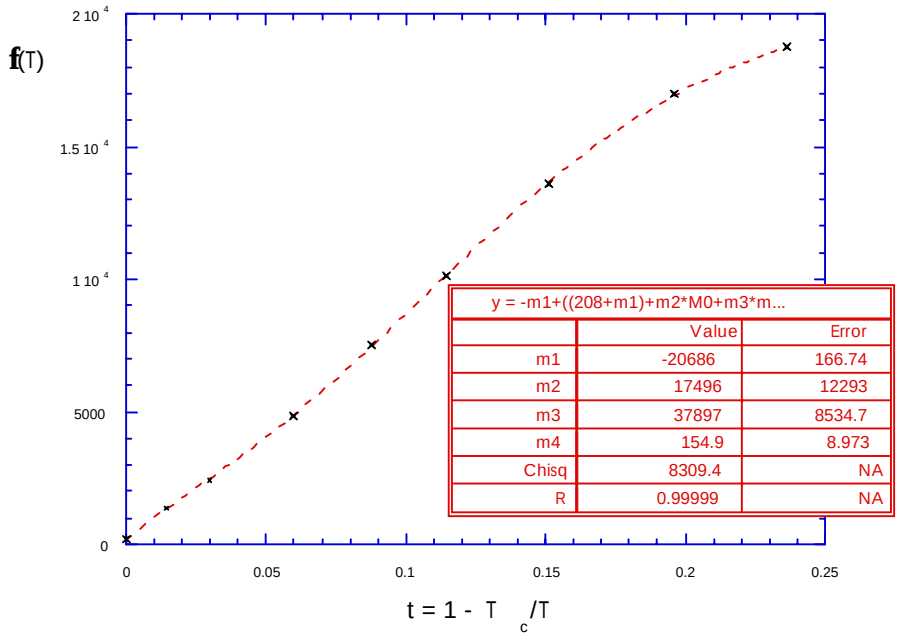

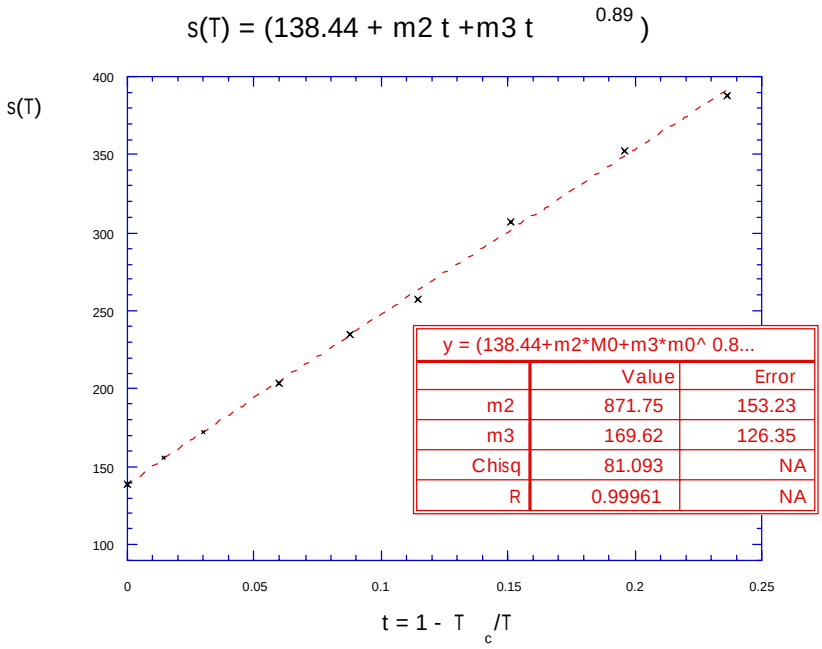

Plots of Π, s, and f for ethane.

The following graphs show the corresponding results for methane. These fits required more corrections to scaling than the corresponding quantities for carbon dioxide and ethane.

Methane

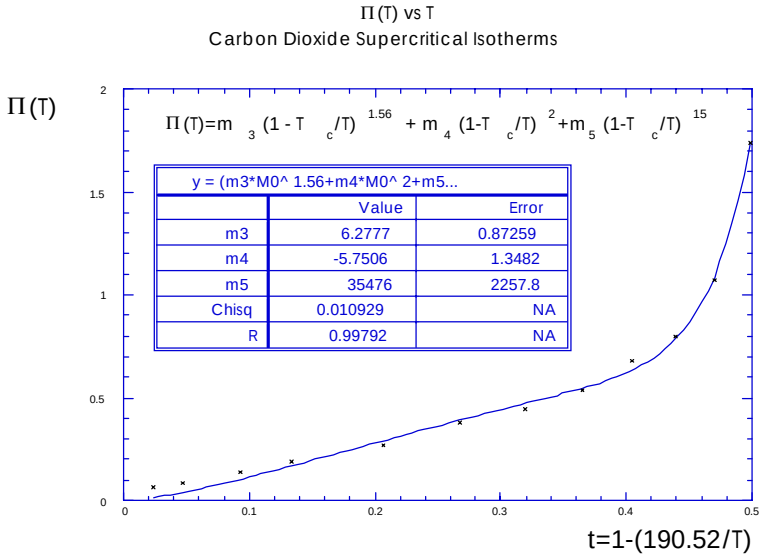

$$f(T) = -m1+\{(208+m1) + m2\ t +m3\ t^{0.89}\}/\{1+ m4\ t^{3}\}$$

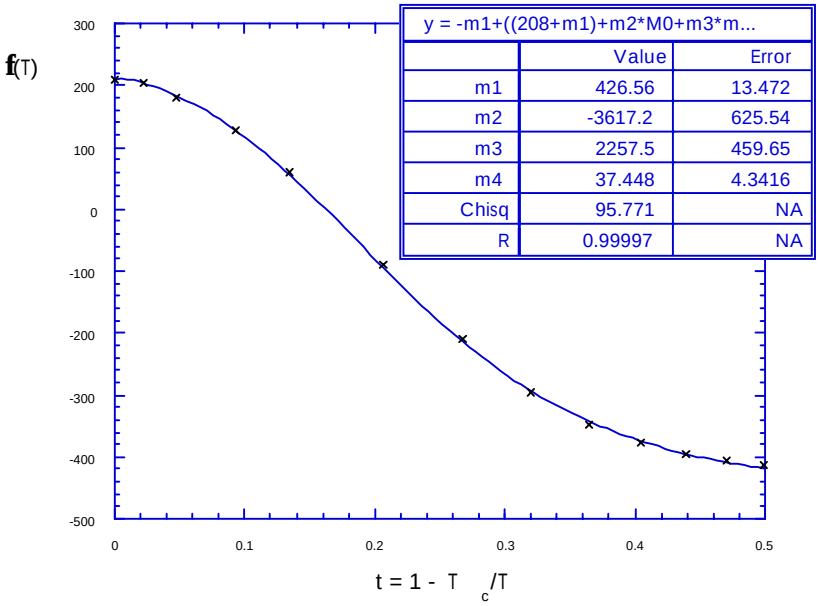

$$s(T) = (97.8 + m2\ t +m3\ t^{0.89})(1 + m4\ t^{3})$$

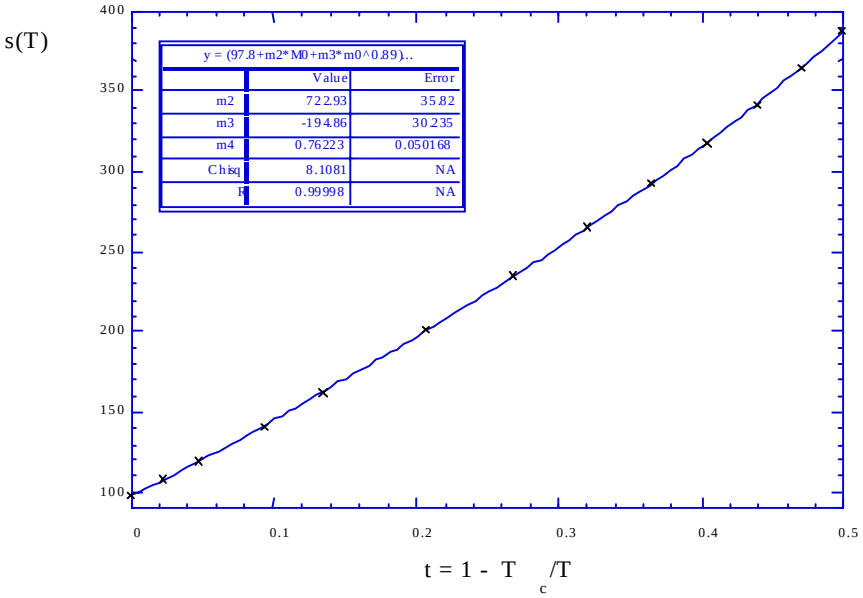

Plots of Π, s, and f for methane

Having functional forms for the parameters Π(T), s(T), and f(T), we can then generate isotherms for

any temperature. The figures below show supercritical isotherms for carbon dioxide. The pressures are in bars and the volumes are in cubic centimeters.

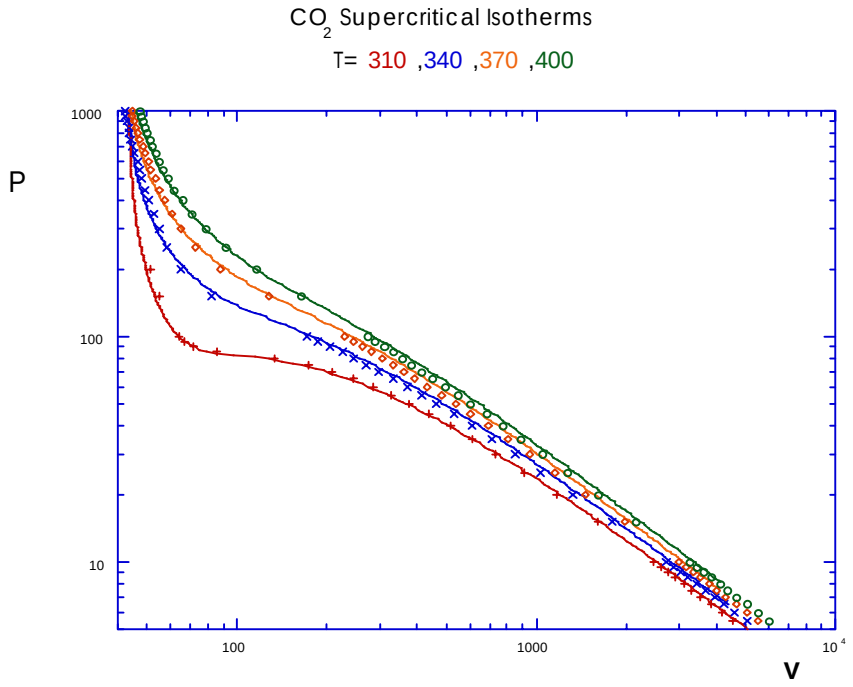

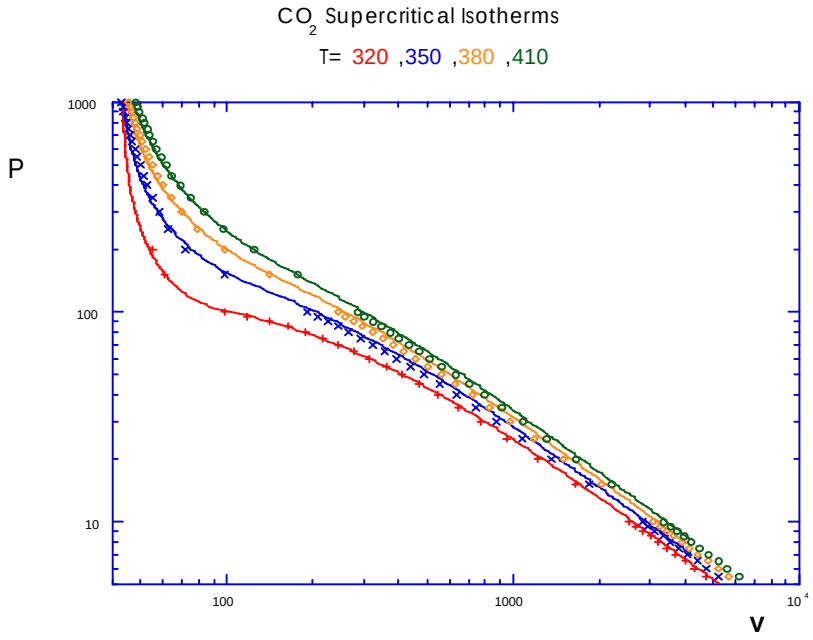

Supercritical isotherms for carbon dioxide

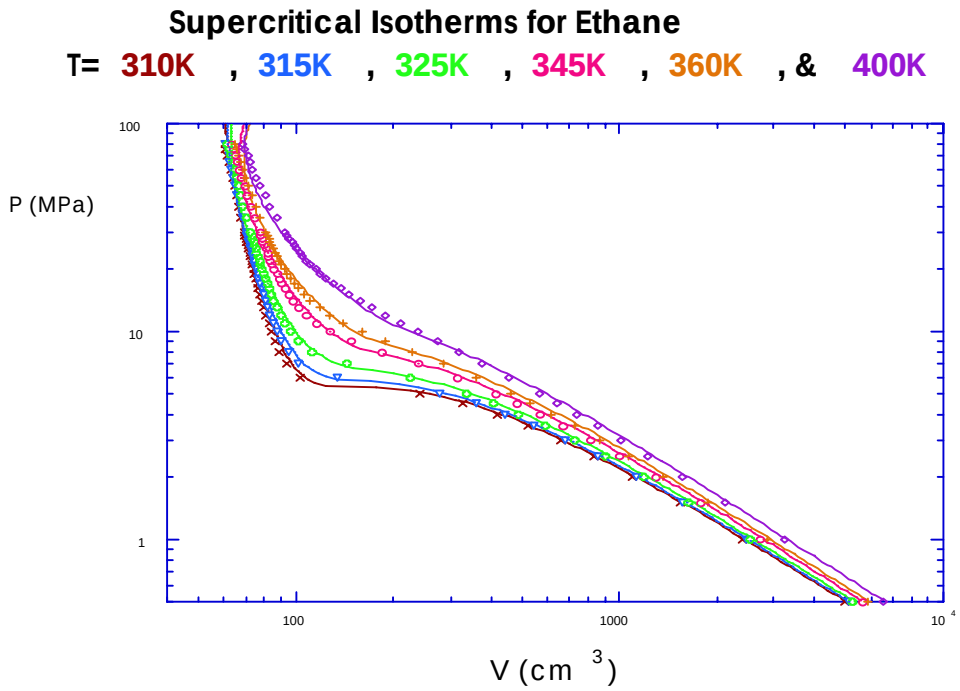

Use of these functions for the fitting parameters leads to the following fits to the supercritical isotherms for Methane.

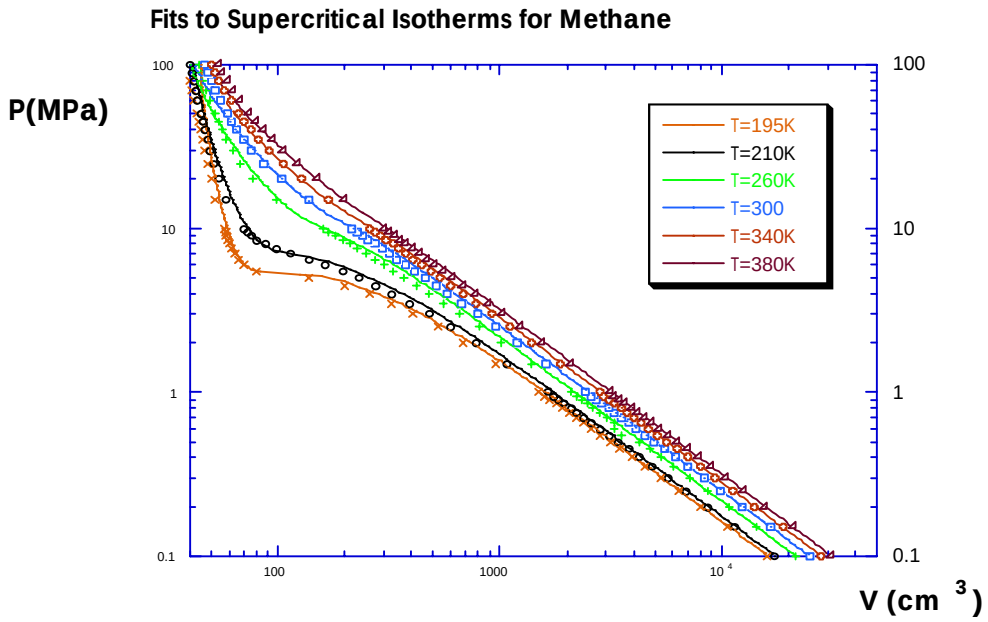

The analysis presented above presents a new method for extending critical behavior to predict reliable supercritical isotherms not only in the critical region, where cubic equations are seriously incorrect, but also in the full parameter space. Although the work presented here used the critical isotherm to determine several of the parameters for fitting the supercritical isotherms, this is not a restriction on the approach. The same equation could be used to fit any near-critical isotherms, thereby determining the fitting

parameters, which seem to be independent of temperature (or at worst weakly temperature dependent). It should be emphasized that with the fits to the temperature dependencies of Π(T), s(T), and f(T), our equations become fully predictive; our procedures will predict the supercritical isotherm for any supercritical temperature.

NATURAL GAS AND NATURAL GAS HYDRATES

BACKGROUND. Methane in natural gas hydrates represents a potentially enormous gas resource with estimates for the U.S. ranging on the order of 9×10^{15} m^3 (300,000 trillion ft^3). This is many times the estimated total of conventional oil and gas resources (Collett, 1995; Sloan and Dendy, 1998). Safe, economic production of this resource will require the development of technology suitable for the challenging environments in which it is found, namely permafrost regions and in sea bottom sediments.

Methane from hydrates can be produced by thermal stimulation, depressurization, or addition of inhibitors or other species that displace equilibrium conditions in the reservoir (Sloan and Dendy, 1998). In areas with favorable geology, the most viable method for gas production from hydrates may involve withdrawal of free gas from a reservoir in contact with the hydrate-bearing strata. As the pressure decreases at the hydrate/free-gas interface, the hydrate decomposes, releasing the gas contained in the hydrate into the reservoir. As this occurs, the temperature at the hydrate/free-gas interface will decrease to the new hydrate equilibrium temperature at the pressure of the interface. The temperature difference between the surrounding strata and the dissociation interface results in the flow of heat to the hydrate at the interface. The rate of heat transfer is related to the thermal conductivity and the temperature gradient that is established. The rate at which hydrate can decompose is, therefore, proportional to the energy transferred by this heat flow. Accurate prediction of hydrate production via depressurization therefore requires an understanding of the equilibrium phase behavior relationship as functions of pressure and temperature in the environment in which the hydrate exists and an understanding of the thermal conductivity of the formation. Recent monographs on gas hydrates have noted the importance of research on obtaining thermal conductivity data for hydrate and hydrate-containing sediment and illustrate the small amount of data available for this property (Makogen, 1997; Sloan and Dendy, 1998). This information is especially important for engineering calculations and economic studies.

Preparation, and Characterization of Gas Hydrates

Chemical potential of gas hydrate is a function of temperature, pressure, concentration of thermodynamic inhibitor, and the size of limited geometry. Equations for integration paths of fixed pore size and solution concentration of the liquid phase has been suggested for temperatures greater than the quadruple point (the temperature, T_q, and pressure, P_q at which all four phases, ice, aqueous phase, hydrate, and gas, reach equilibrium). For temperatures below the quadruple point, only conditions of bulk hydrates in equilibrium with pure ice have been considered, since the equilibrium under conditions below the quadruple temperature should be independent of either the pore size or the inhibitor concentration.

This work expands the thermodynamic equations to integration paths that join two states, which are not only of different pressure and of temperature, but also in different liquid phase concentrations and of different pore sizes. In particular, integration between two states was examined: a) a state in which both temperature and

pressure are at the commonly chosen reference point of T_0 = 273 K and P_0 = 0 MPa, but with finite pore size and non-zero inhibitor concentration; and b) a state with its temperature below the quadruple point temperature.

Ethane with a minimum purity of 99.95 mole % was obtained from Matheson. Nitrogen desorption and adsorption studies using Quantachrome Corp Autosorb-1 equipment were used to determine the pore size distribution (Ferer, Sams, Geisbrecht, and Smith, 1993) and pore volume of each of the silica gel samples used in the experiments. The silica gel samples, without any further treatment, were placed in a desiccator containing degassed, distilled water for a period of about 7 days to prepare silica gel with sorbed water. The silica gel powder for each cell was mixed with 5-mm diameter glass beads and loaded into the cells. The cells were then closed and tested for leaks at 13.09 MPa for 24 hours. Nitrogen gas was then very gently released as the cell was gradually cooled down towards 243K. During the above course, the combination of the cell temperature and nitrogen pressure was maintained so that the samples were outside of the phase stability zone for bulk nitrogen hydrate. The cell was evacuated to less than 25 torr for 50 minutes to remove residual air and nitrogen gas from the cell after the cells had been cooled to 243 K. At 243 K, each cell was gently rotated upside-down to enhance the dispersion of silica gel grain onto the internal surface of the cell and to the surface of the glass beads. The total volume of glass bead used in each cell has been listed in Table 1. The headspaces of each cell were calculated by subtracting the volume of silica gel saturated with water and that of the glass beads from the total volume of the enclosed cell space.

Table 1. Sample Specifications

Cell # (Sample Name)	1 (2nm)	2 (3nm)	3 (5nm)	4 (7.5nm)
Volume of the cell*, cc	59.8	68.7	68.1	68.7
Net weight of silica gel saturated with water, g	15.8	16.54	14.64	10.33
Density of try silica gel, g/ml	0.6196	0.4898	0.4327	0.4057
Volume of sample, cc	25.5	33.8	33.8	25.5
Volume of glass beads, cc	14	12.5	19.6	18

*includes the space of the connecting tubing and the valves.

For all the cells, hydrate formation was initiated at 243 K by charging the cells with ethane up to 0.689 MPa (100 psi), a pressure lower than the vapor pressure of liquid ethane at that temperature (dew point pressure is approximately 1.06 MPa). Significant pressure drop was observed for all the cells, and the gas was recharged several times until the gas absorption process became very slow. The cells were then charged to a higher ethane pressure of 1.24 MPa, and the samples were allowed to stand for further hydrate formation for 36 hours. Then the ethane pressure was slowly brought down to around 0.96 MPa, a pressure below the dew point pressure of ethane. At this point, the system pressure for each cell was seen to be stabilized, i.e., no pressure change was observed for more half an hour for the 2, 3 and 7.5-nm samples, and only a 1 psi pressure drop was observed for the 5-nm sample after 30 minutes. After hydrate formation, each sample was evacuated to remove extra ethane, and all the samples were allowed to reach equilibrium.

The pressure measurements were made with pressure gauges of two different scales and were accurate to 0.67 psig (0.004595 MPa).

Results on the ethane hydrate in 3, 5, and 7.5-nm silica gel samples reveals that when the temperature

is sufficiently low, the equilibrium pressure of gas hydrate is independent of the pore size of the porous media. This is the first time that the pore size independence of equilibrium pressure has been revealed. No experiment had previously been successfully performed in the temperature range well below the quadruple point of gas-ice-hydrate-water four-phase equilibrium of pore hydrates. The fact of pore size independence was clouded by the pore size distribution of the porous media. In these porous media there are always pores that are too small in which to form pore ice. At temperatures low enough to establish ice-hydrate equilibrium in most pores, hydrate could still be at equilibrium with liquid water in these small pores. During the stepwise temperature increase process of the phase equilibrium measurement, the dissociation of hydrate in the smaller pores leads to higher equilibrium pressure than that based on ice-hydrate equilibrium. To reveal the ice-hydrate equilibrium, it is necessary to remove the remaining water-hydrate equilibrium. This was done by carefully dissociating gas hydrate in the smaller pores that still contained liquid water while preserving the hydrate-ice equilibrium in bigger pores. Preparing sufficient amounts of ice in the bigger pores and maintaining sufficient lower system pressure achieved this goal. At a given temperature well below 273 K, the system pressure should be chosen such that it is higher than the equilibrium pressure for hydrates in most pores but lower than that required to keep hydrate stable in small pores. As a result, hydrate dissociation took place in the small pores. The ethane molecules thus released further pump up the system pressure and then form hydrate in the big pores. When the final equilibrium is reached, the only equilibrium left should be the ice-hydrate equilibrium, with its equilibrium pressure being a pressure independent of the pore size. It is interesting to find that as long as the equilibrium is between ice and hydrate, the equilibrium pressure is the same, regardless of the size of the pore in which the hydrates reside. A paper describing this research has been submitted to the journal, Langmuir.

The shape of the equilibrium pressure and temperature curve depends on how hydrate is distributed in pores of various sizes. The point where the P-T curve of the porous sample diverges from that of the bulk sample indicates the temperature and pressure at which the last hydrate-ice equilibrium is broken and replaced by hydrate-water equilibrium at the same time. The hydrate at this equilibrium must have resided in pores that are the smallest among those that host hydrate-ice equilibrium, and the smallest that ever hosted a hydrate-water equilibrium, i.e. a critical pore size, r_c.

If the temperature of the system further rises by δT, to $T+\_\delta T$ from this point, either hydrate in pores of the critical size will all dissociate, or some of them will remain and support a new hydrate-water equilibrium at $T+\_\delta T$ by generating a pressure higher than the equilibrium pressure at T. For the former, the increase in pressure will be contributed by hydrate dissociation from the next smallest pores. For the latter, further pressure increases will only affect hydrates in pores of this critical size until the system reaches a new equilibrium, which can only be at the hydrate-water equilibrium. No hydrate dissociation should take place elsewhere, since the new equilibrium pressure will be higher than the dissociation pressure of hydrate in the rest of the pores, which are larger in diameter.

The higher equilibrium pressure of hydrate in small pores is due to the surface tension effect and can be interpreted from the point of view of intermolecular forces. Mechanical pressure exerts an additional force on water molecules. This force keeps water molecules together, i.e., the force serves as a resistance to the vaporization of water. Surface tension also exerts a tensile force between water molecules on the surface of a liquid water droplet. The tensile force acts in an opposite direction, separating the water

molecules from each other and facilitating vaporization. The surface tension effect can be evaluated in terms of chemical potential reduction compared with the chemical potential of water in a bulk condition, since,

$$-\frac{2\sigma}{r}\cos\theta = P_l - P_g \quad (1)$$

Where σ is the surface tension; r is the radius of a pore or a water droplet; υ is the contact angle; P_l is the real pressure on the surface of the pore water; and P_g is the gas pressure that equals the surface pressure of bulk water. Assuming pure water:

$$-\frac{2\sigma V_l}{r}\cos\theta = V_l(P_l - P_g)$$
$$= RT\ln(\frac{f_l}{f_g})$$
$$= RT\ln a$$
$$= (\mu)_{pore} - (\mu)_{bulk} \quad (2)$$

and,

$$(\Delta\mu_w)_{bulk} = (\Delta\mu_w)_{pore} - \frac{2\sigma V_l}{r}\cos\theta \quad (3)$$

where,

$$\Delta(\mu)_{pore} = \mu_\beta - (\mu)_{pore}, \quad (4)$$

and,

$$\Delta(\mu)_{bulk} = \mu_\beta - (\mu)_{bulk} \quad (5)$$

and μ is the imaginary chemical potential of the empty cage. For the bulk condition, it has been established that, in bulk,

$$\frac{\Delta\mu_w^0}{RT_0} - \int_{T_0}^{T_F}\frac{\Delta h_w}{RT^2}dT + \int_{P_0}^{P_l}\frac{\Delta v_w}{RT_F}dP - \ln(\gamma_w X_w) + \sum_i \nu_i \ln(1 - \sum_k y_{ki}) = 0 \quad (6)$$

since from van der Waals and Platteeuw [2,3],

$$(\Delta\mu_w) = (\Delta\mu_H) \quad (7)$$

while $(\Delta\mu_H) = \mu_\beta - \mu_H$, and μ_H is the chemical potential of hydrate, and

$$(\Delta\mu_H) = -RT\sum_i \nu_i \ln(1 - \sum_k y_{ki}) \quad (8)$$

and

$$\frac{(\Delta\mu_w)}{RT} = \frac{\Delta\mu_w^0}{RT_0} - \int_{T_0}^{T_F}\frac{\Delta h_w}{RT^2}dT + \int_{P_0}^{P_l}\frac{\Delta v_w}{RT_F}dP - \ln(\gamma_w X_w) \quad (9)$$

Accordingly, in porous media,

$$\frac{\Delta\mu_w^0}{RT_0} - \int_{T_0}^{T_F} \frac{\Delta h_w}{RT^2} dT + \int_{P_0}^{P_l} \frac{\Delta v_w}{RT_F} dP - \ln(\gamma_w X_w) + \sum_i v_i \ln(1 - \sum_k y_{ki}) = -\frac{2\sigma V_l}{rRT} \cos\theta \quad 0 \quad (10)$$

The additional term on the left of Equation (10) requires higher-pressure input to the term of $\sum_i v_i \ln(1 - \sum_k y_{ki})$ 0 on the left to balance the equation. The increase in pressure causes an opposite effect from the term $\int_{P_0}^{P_l} \frac{\Delta v_w}{RT_F} dP$ 0, which can be overcome, however, since the rate of the increase per unit pressure change is greater in the former than the latter.

Equation (10) defines a pressure-temperature relationship for a given pore radius. Comparing this relationship for a radius *r* that falls in the range of pore size of the silica gel sample with an experimentally measured *P-T* curve, one can find an intersection at some pressure and temperature. The equilibrium in the sample under question for this pressure and temperature is therefore between liquid water and hydrate residing in a pore of radius *r*. Porous silica gel consists of pores with a spectrum of radii. A set of intersection points (*P, T*) can be determined for a radius *r*. The pressure difference between two adjacent points gives the mole number of ethane contained in pores between the two corresponding radii. The shape of the experimental *P-T* curves is therefore affected by the relative amount of the hydrates stored in the pore of each pore radius.

The gas hydrate laboratory was moved from B25-208 to B2-42 to make room for a new Computer Laboratory. Gas sensors and outdoor gas cylinder cabinets were installed in the new location before the transfer of equipment. After completing the planned work on single gas hydrates, it was decided to investigate the preparation and characterization of binary hydrates of gases in natural gas.

A system for the preparation of mixed gas hydrates in porous media and for on-line gas chromatographic (GC) analysis of the relative concentration of components in the gaseous mixture in equilibrium with hydrate/ice or hydrate/water was assembled in the new location. The hydrate cell was modified to facilitate the transfer of a gaseous mixture to the GC. A HP 5890 GC equipped with a flame ionization detector was selected for GC analysis. The hydrate cell and the GC were interfaced via uncoated quartz tubing and a manually operated 6-port valve with a 10-L loop. A packed column (Supelco® SP2100) was used to separate carbon dioxide from propane. A shakedown experiment was carried out, and all the components performed as expected. However, the technique used to transfer the gas mixture from the hydrate cell to the GC and to inject a standard gas to the GC had some faults. These imperfections were corrected by using a Valco microvalve in the transfer line and by transferring the standard gas to the GC in the same manner as the experimental gas mixture. After setting up the apparatus, the first experiment was the preparation and characterization of the binary hydrate of propane and methane. Propane was introduced into the cell maintained at 267.5 K at 60 psig. After the formation of the hydrate was completed, the bath temperature was lowered gradually to 261 K. As in previous experiments, the cell was left at this temperature for a long period. Formation of the hydrate/ice/gas equilibrium was noted visually. Then methane was introduced into the cell at 1650 psig, and enough time was allowed for the formation of methane hydrate. The new hydrate/ice/gas equilibrium was established at 261.0

K. After the system reached equilibrium, the gas mixture was transferred from the hydrate cell to the GC, and the chromatogram was recorded, which displayed two signals, one due to methane and the other due to propane. The former was more intense than the latter, because the partial pressure of methane in the hydrate cell was much higher than that of propane. Then the cell temperature was increased in increments of 2 K, the new equilibrium was established, and the gas sample was analyzed at each temperature up to 290 K. As the temperature was changed, there were increases in the intensity of the propane signal, but not in that of methane. This suggests either that no methane hydrate was formed or that methane hydrate was formed and since the initial concentration of methane was too large, the GC failed to recognize the increments in the concentration of methane with temperature. Our experiments with the binary hydrate of propane and carbon dioxide indicate that the latter is the most probable explanation. After completing the work on the binary hydrate of propane/ethane and carbon dioxide, a methane/propane system will be re-examined with some modifications to the apparatus.

Before the present work on binary hydrates was started, an experiment was carried out with propane and carbon dioxide, using a procedure analogous to the method mentioned above, in which there was definite evidence for the formation of the hydrate of carbon dioxide along with that of propane. Therefore, it was decided to investigate the binary system containing propane and carbon dioxide, instead of continuing the investigation of the methane/propane system. Since flame ionization detectors are not capable of detecting carbon dioxide, a thermal conductivity detector was added to the GC.

The binary hydrate of propane and carbon dioxide was produced using the procedure detailed above in silica gel of 5-nm pore radius. There was a rapid drop in the cell pressure, indicating the formation of the hydrate of carbon dioxide. The cell was repetitively re-pressurized until the drop in the cell pressure was marginal. Then the new high phase equilibrium was established, and the chromatogram was recorded. Data were collected at intervals of 1 K till the decomposition of the hydrate was complete. In addition to recording the GC of the binary mixture, the chromatogram of pure carbon dioxide and propane was recorded to check the performance of the instrument.

The number of moles of carbon dioxide and propane in the gaseous phase was calculated from the integrated intensity of the GC peaks and the weight factors for the two gases. There was some scatter in the data. Therefore, it was decided to fit the data to a polynomial function and estimate the accuracy of the measurements. The software named MATLAB® was used in this calculation, and the mole fraction of the two components was obtained from the fitted data.

In the work on single hydrates, the equilibrium fugacity was obtained using the second virial coefficients. In the present work, it was calculated directly from the Peng-Robinson equation of state.

Equilibrium pressure- temperature data were obtained for the other (7.5-, 3.0-, and 2.0-nm) pore sizes, and data analyses were completed. All the results were not as expected. The equilibrium pressure-temperature data for the 7.5- and 5.0-nm silica gel samples were comparable because the pore size distribution in these two samples are nearly identical. The equilibrium pressure for carbon dioxide in 3-nm silica gel was shifted upward, as observed in the work on single gases. However, an analogous shift was not observed in the equilibrium pressure for propane hydrate in the 3-nm silica gel. The data for the 2-nm silica gel was also surprising. The data will be fitted into a model, and the modeling work may explain some of the anomalies.

Although there is no crystallographic evidence, apparently the crystalline structure of water is sII for the double hydrate with propane and carbon dioxide. SII is a body-centered cubic lattice in which each cell contains 8 large cages, 16 small cages, and 136 water molecules. The propane molecules can occupy all the large cages, leaving the small cages for carbon dioxide. Because a large number of cages are available for carbon dioxide, the hydrate of carbon dioxide is formed with ease as evidenced by the rapid drop in the cell pressure when carbon dioxide is admitted into the cell. Estimation of the number of molecules of propane and carbon dioxide per 136 molecules of water will provide a better proof for the sII structure of the double hydrate.

The hydration number of the single gas hydrates was derived using the hydrate cell volume of the glass beads, initial and final pressures, etc., and an equation of state corrected for the non-ideality of the gas with the second virial coefficient. The second virial coefficient for the binary mixture was calculated using some published thermodynamic data, and the total number of gas molecules in the sII structure was calculated for all four pore sizes. This number was close to 24, suggesting that gas molecules occupy all the small and large cages. An alternative method is now available for estimating the molecular structure of the binary hydrate. These two methods will be modified and tested.

Preparation and characterization of the binary hydrate of carbon dioxide and ethane was started with silica gel of 7.5-nm pore size. As in the previous experiments, the hydrocarbon was introduced into the cell first, and then carbon dioxide was added. The equilibrium pressure-temperature data were collected and analyzed in the usual manner.

We are postulating that the hydrate structure with ethane and carbon dioxide is sI, which is also a body-centered cubic structure, and that each cubic cell contains 6 large cavities, 2 small voids, and 46 molecules of water. It appears that the large cavities are filled with ethane and the small cavities with CO_2. This hypothesis is yet to be proved. However the equilibrium pressure-temperature plot of propane-CO_2 along with that for ethane-CO_2 suggests that the two binary hydrates are in different structures. The hydration number, which is yet to be estimated, may shed some light on the molecular structure of ethane-CO_2 hydrate.

The enthalpy of dissociation of pore and bulk hydrates into ice and gas and into liquid water and gas is customarily calculated using the Clausius-Clapeyron Equation. Enthalpy for an equilibrium process, such as the dissociation of hydrate into ice and gas, can also be calculated using free energy functions. The enthalpy of dissociation for the hydrate of carbon dioxide in different pore sizes was calculated. The results will be included in a report on the hydrates of carbon dioxide.

Production of Natural Gas Associated with Hydrates: Formation and Dissociation Kinetics of Methane Gas Hydrates

In the past, several investigators have studied the thermodynamics and crystal structures of natural gas hydrates. However, the reaction engineering kinetic data of formation and dissociation of methane gas hydrates (MGH), together with heat and mass transfer considerations, have not yet been clearly established experimentally, and only scattered qualitative kinetic data obtained under limited conditions have been published. Therefore, a systematic study of the reaction engineering kinetics of formation and dissociation of MGH has been undertaken.

The study of reaction engineering overall reaction rates of formation and decomposition of MGH within several well-defined synthetic sediments was accomplished by using our custom built high-pressure batch and

semi-continuous reactors (patent application in process). These synthetic sediments are very well defined in terms of their powder packing structures and chemical surface characteristics. The formation of gas hydrates is an exothermic reaction that is carried out at high pressure and low temperature (273.5 K). The decomposition of hydrates is an endothermic reaction that is carried out at pressures below the equilibrium pressure specified by the three-phase diagram. Decomposition of hydrate was accomplished through a controlled depressurization technique starting at a pressure of 2.7 MPa, maintaining the temperature constant at 273.5 K.

Overall kinetic rate constants for both the formation and decomposition reactions were determined from experiments, including the overall order of the reaction, by using several different sediments. Based on the experimental results, we obtained a reaction engineering rate equation of the quasi-first order type for the formation reaction where the rate constant k_f is practically a function of the pressure, temperature, sediment type, and sediment catalytic reactivity. During decomposition, two types of rate behavior were observed depending on the type of sediment used. In some cases, the order of decomposition reaction was of a zero-order, while in other cases it was of a first order.

For production of natural gas, it is important to understand how to control the decomposition rates of natural gas hydrate samples by depressurization. In the past, decomposition rates were not studied by depressurizing but by changing temperature, i.e., Bishnoi (1983), Englezos (1987), and Kim et al. (1987). The decomposition was accomplished by increasing the temperature at a certain pressure. In studies by the above investigators, the reaction system consisted of either [CH_4(g) - H_2O(l) - MGH(s)] or [CH_4(g) - H_2O(l) - H_2O(s) - MGH(s)], in contrast to our model reacting system, which consisted only of [CH_4(g) - H_2O(l) - sediment - MGH(s)].

In addition to the MGH system, the formation and dissociation rates of propane gas hydrates (PGH) were measured at a temperature of 273.5 K and a pressure of 48 psig under the condition of using the phase system of propane (s), water (l), and propane gas hydrate (S).

Using the custom-designed structured granules of sediments of several materials, homogeneously reacting solid-state packed bed reactors were designed and operated in batch mode and/or continuous mode. For the formation reaction of clathrate compounds of MGH, the reaction rate equation was developed in terms of reaction engineering from experimental data and, the order of the chemical reaction was found to be unity. Reaction rate constants were obtained that could be controlled by the selection of the sediment property and operating condition.

For the dissociation (decomposition) reaction of MGH, the reaction engineering rate equation was developed from experiments. The order of the reaction could be controlled by appropriately adjusting the granule property.

As the effect of the property and amount of sediments on MGH dissociation rates could reproducibly be investigated in the laboratory by the method proposed in this paper, the assessment of natural gas hydrate resources in the strata in the gas field would be accomplished efficiently.

Properties of Natural Gas Hydrates

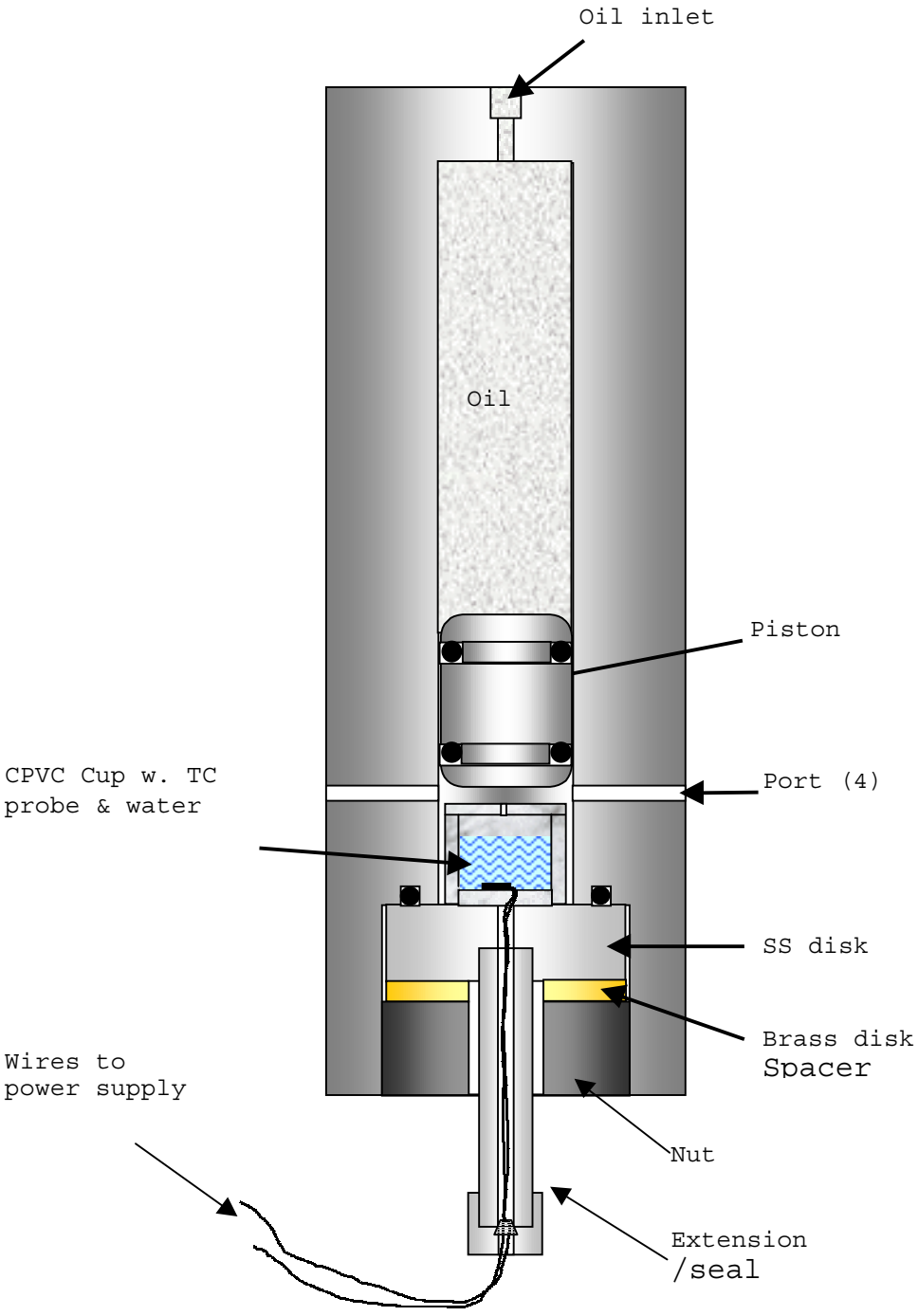

The experimental work is performed inside a high-pressure variable-volume view cell (HVVC) that has been configured to contain a specially designed thermal conductivity (TC) probe. A diagram of the HVVC with the TC probe assembly is shown above. In a typical experiment, hydrate is formed from a gaseous hydrate former, such as methane, and water in a manner that allows the hydrate to be in contact with the TC probe. The TC probe is approximately 3 mm square and consists of a commercially available thin foil heater that is made by depositing a narrow strip of nickel in a serpentine pattern on a Kapton substrate. The exposed surface of the foil is covered with a layer of Kapton, resulting in a robust, flexible heating element with an overall thickness of less than 50 µm and a working temperature range of -200 to +200 C. The thermal properties

of a substance in contact with the heating element are measured by passing a current through the heater, which increases its temperature. Since the thermal properties of the specimen govern the heat loss from the heater, these properties can be obtained by analyzing the temperature history of the heater. The heater temperature is measured indirectly by measuring the resistance of the foil strip and by using the known temperature coefficient of resistivity of the nickel.

In FY 2001, the design and operation of the HVVC were modified to enable more reliable detection of hydrate formation from the pressure and temperature data recorded during an experiment. The goal of the redesign was to maximize the amount of water in the cell and minimize the quantity of gas so that when hydrate formed, the change in the pressure associated with gas uptake would be easily observed in the pressure data. In the previous configuration, the drop in pressure could not be observed owing to too little water and too much gas.

The major changes included the following: 1) making a larger sample cup to hold more water; 2) making the sample cup, including base and lid, occupy a larger portion of the volume in the HVVC; 3) eliminating any unnecessary connecting tubing; 4) shortening as much as possible the tubing leading from the ports on the cell to the pressure transducer and gas inlet/outlet valve; and 5) operating with the piston as far down as possible to minimize the available gas volume in the cell.

The physical connections to the TC probe and its attachment to the HVVC were also modified to permit easier installation and reuse of the probe and sample cup. The TC probe is located in a small CPVC/PVC cup that is mounted onto a specially machined stainless steel disk that incorporates a commercial fitting designed to seal the electrical leads in the high-pressure environment. Water is placed into the CPVC cup, and the cell is filled with methane gas. The movable piston can be used to compress the gas as required.

The total amount of water used in the sample cup was also a factor. The layer of water over the TC probe has to be thick enough to give meaningful data, but not so thick as to prevent hydrate formation throughout its mass. The final design has the cell holding from between 0.25 ml to 1 ml of water.

A sample cup, similar to that which held the TC probe, was made with a transparent bottom so that hydrate could visually be detected. This cell was used with 0.25 ml of water, which had been purified by reverse osmosis and ion exchange, and methane to observe hydrate formation under conditions similar to those that would be used in experiments with the TC probe. Hydrate formation was observed at pressures near 4000 psig, 2600 psig, 1200 psig, and 750 psig; however, at the lowest pressure hydrate would not always form. Figure 2 depicts pressure-temperature data obtained near 1200 psig. Three separation cycles of hydrate formation and decomposition are shown. A variable amount of subcooling that ranged from 2.9 ^{o}C to 7.6 ^{o}C was required, as evidenced by the different onsets of pressure decrease during hydrate formation. The decomposition cycles were highly reproducible and verify that the experiments were producing the anticipated hydrate phenomena relative to that previously observed in the literature (Sloan and Dendy, 1998). No liquid water was visually observed in the sample cup after hydrate formation; however, this is not conclusive evidence that all of the water was incorporated into the hydrate lattice.

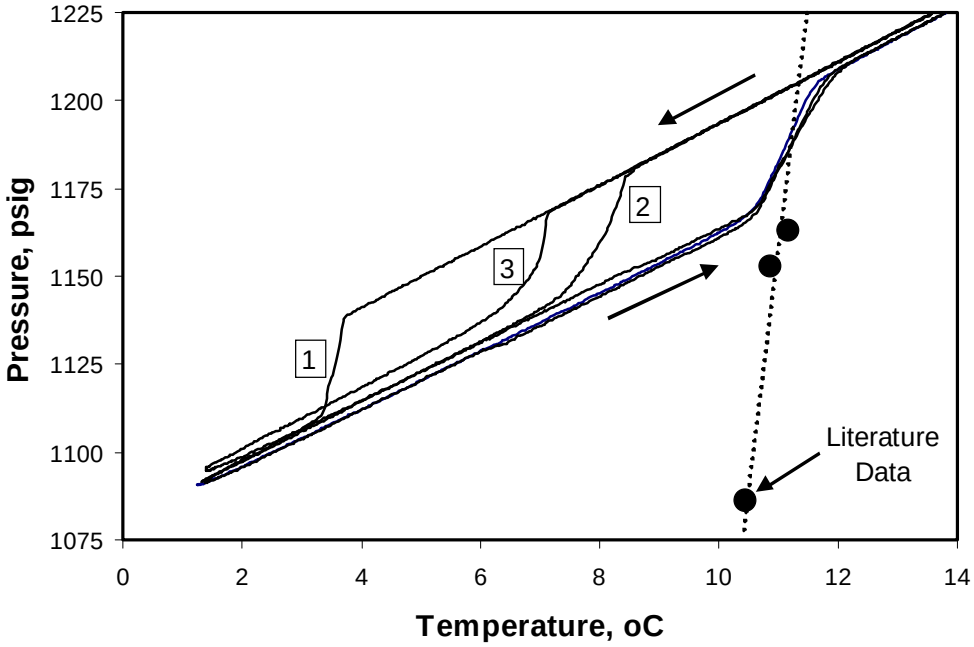

Figure 2. Summary of methane hydrate formation experiment with new sample cup. No TC probe was used in this experiment. The solid circles represent phase behavior data of others.[2]

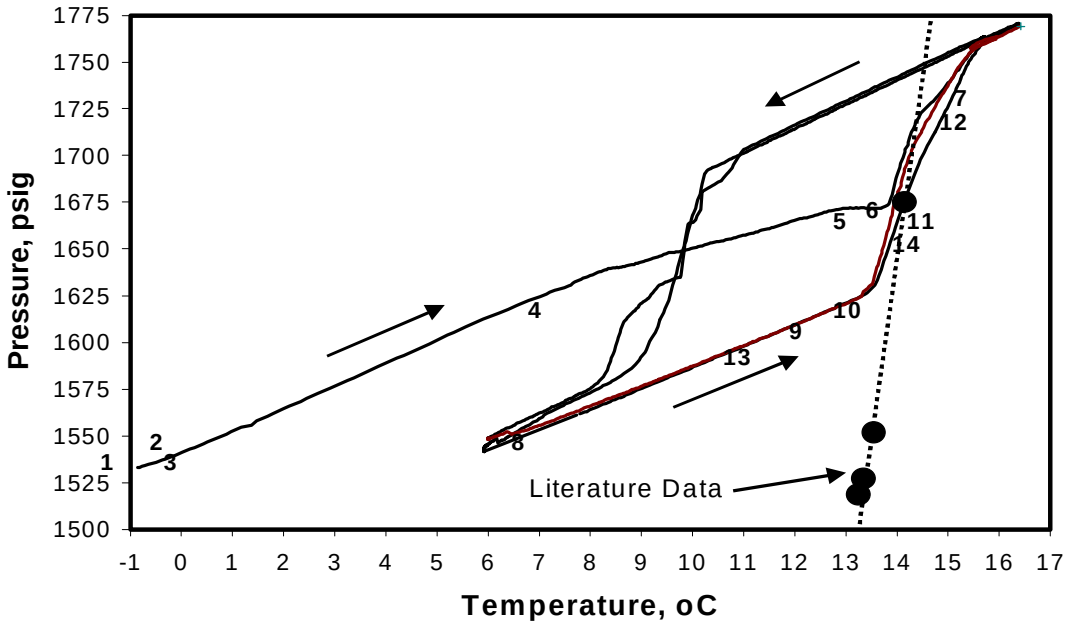

Figure 3. Summary of methane hydrate formation experiment using the TC sensor. Numbers indicate thermal conductivity measurements that are described in the text.

A similar experiment was performed using the sample cup with the TC probe. In this instance, 1.00 g of water was placed into the cup. Hydrate formation and decomposition were observed near a pressure of 1700 psig. Figure 3 depicts the pressure-temperature data from this experiment along with a summary of the results of thermal conductivity measurements.

Before starting the hydrate formation and decomposition cycle, ice was formed in the sample cup with the HVVC filled with helium. This was done to verify the formation of ice and that the water remained in the sample cup. The measured thermal conductivity of 1.6 W/m-°C at Point 1 in Figure 3 (-1.5°C) is consistent with nearly pure ice (a small amount of dissolved or entrapped helium was likely still present).

Immediately upon adding methane and pressurizing, the conductivity dropped to about 0.75 W/m-°C (point 2), possibly indicating some hydrate formation, and dropped further when held overnight at nearly constant temperature (point 3, k = 0.25 W/m-°C). The initial pressure trace makes it clear that some hydrate did form during this initial cycle starting from ice. The conductivity continued to drop as the temperature was raised (points 4 and 5), but rose suddenly (point 6, k = 0.43 W/m-°C) just before the onset of decomposition was detected in the pressure trace. At point 6, the conductivity was a little lower than, but consistent with that of water.

Similar trends were observed in the first complete cooling/heating cycle (points 8 to 14), with values even more consistent with the conductivity of water observed at points 10 and 11. At points 6 and 10, the increase in thermal conductivity can be detected before any clearly defined pressure increase associated with hydrate decomposition occurs.

These results show that the goals of improving the ability to detect the formation and decomposition of hydrates in the view cell from the pressure-temperature history and improving the TC measurement protocols have been achieved.

Computer Modeling Activities

Computer simulations of hydrate dissociation in natural reservoirs were performed. For a one-dimensional case when the well pressure is constant, a numerical method was developed to solve the general governing equations. A manuscript was prepared on natural gas production from hydrate dissociation using the linearization method of Makogon and accepted for publication in the Journal of Chemical Engineering Science. A manuscript related to the hydrate dissociation in an axisymmetric reservoir was also prepared and submitted for publication.

Modifications were made to the NFFLOW simulator. NFFLOW is a discrete-fracture, single-phase, single-component reservoir simulator originally intended for the study of naturally fractured gas reservoirs. It was developed as an alternative to conventional dual porosity/permeability simulators when issues such as connectivity, clustering of fractures, or anisotropy of fracture flow are important.

The feature that distinguishes NFFLOW from conventional simulators is that NFFLOW conceptualizes the behavior of naturally fractured reservoirs as resulting from the interaction of a set of highly conductive flow

paths (the fractures) and a set of source/sinks that can supply gas to or receive gas from these flow paths (the rock matrix). The source/sinks are referred to as recharge models, but it should be remembered that these models can either supply or receive gas depending on the local pressure gradients. Each fracture that is modeled by the simulator is divided into segments by its intersection with other fractures or a well bore. Two recharge models are assigned to each fracture segment in order to represent the reservoir rock on either side of the segment. The recharge models are assumed to supply or receive gas at the midpoints of the fracture segments. These points are called recharge points. The recharge models can be of any form. All that is required of the recharge models is that they calculate the gas flow rate at the face of the rock matrix as a function of the pressure history in the bounding fracture segment. The present configuration uses small one-dimensional unsteady systems as recharge models. These systems will be described in more detail later.

The points where fractures intersect other fractures or well bores are called nodes. NFFLOW is based on solving for the pressure distribution that results in the conservation of mass at all nodes and recharge points. The volumetric flow in the fracture segments is proportional to the local pressure gradient along the fracture and inversely proportional to the gas viscosity. The mass flow rate in the segments is equal to the gas density times the volumetric flow rate. This results in non-linear equations that can be put into linear form by transforming to a variable that is known as the real gas potential in the petroleum industry. In the remainder of this report, this quantity will usually be referred to as the potential. After this transformation, the fracture flow is described by linear equations, but the recharge models still possess non-linear terms. The total set of algebraic equations is solved by means of the Newton-Raphson technique. The resulting linear equations are solved by first eliminating the potential at the recharge points. The reduced set of equations that describes the potential at the nodes is solved by a conventional numerical technique. The method used by NFFLOW to solve this set of linear equations is successive over-relaxation. This method for the linear solver was chosen because the set of equations is sparse but unstructured. The equations are unstructured because of the random nature of the fracture network. After the potential has been calculated at the nodes, the potential at the recharge points is calculated by a simple back substitution. The Newton-Raphson iterates until the material balance error is reduced to a specified tolerance. The recharge models are solved at every Newton-Raphson iteration to insure consistent coefficients in the linear equations.

The well bores are treated in a fashion similar to the fractures except that certain constraints must be applied. The wells in the simulator may be operated under either pressure or rate control. If pressure control is specified, then the well bore potential becomes a known quantity and is removed from the set of unknowns. On the other hand, if a well is rate-controlled, the potentials at well bore nodes remain as unknowns, but there is a constraint that the total flow into the well bore must be equal to the user specified quantity. The code for Newton-Raphson coefficient generation as well as the linear solver contains logic checks to ensure that these requirements are satisfied.

The recharge models are based on the one-dimensional continuity equation. The flow velocity appearing in the continuity equation is calculated using the Darcy equation, and the gas density is expressed in terms of a Z-factor to account for non-ideal effects. This results in a non-linear partial differential equation (PDE) in space and time. The flow terms in this equation become linear when the transformation to the real gas potential is made. The resulting PDE is still non-linear because of the accumulation term, but transformed PDE is more suitable for solution by numerical techniques. The PDE is discretized in space by the control-volume technique and discretized in time using a backward time difference for the accumulation term. This yields an implicit

formulation that is unconditionally stable. The resulting set of non-linear algebraic equations is solved by Newton-Raphson iteration. The set of linear equations solved at each iteration is tridiagonal and solved with minimal work using the Thomas algorithm. Because this is the innermost computational element in the simulator, it is coded for maximum efficiency by tightly coupling the Newton-Raphson coefficient generation and update, as well as the Thomas algorithm, into a single compact subroutine.

The NFFLOW code is logically divided into three parts: the initialization, the control and recurrent data interface, and the solution propagator. The initialization section reads the PVT data and the network definition and generates all the arrays used by the time stepping calculation. The control and recurrent data interface reads the recurrent data that controls the well operation (setting boundary conditions for the simulator) and selects the type and frequency of reports/runtime graphic displays (output). It then computes a time step compatible with the requirements, schedules the specified output, and produces the required output at the scheduled times. The solution propagator section uses the state of the system at the end of the last time step and the boundary conditions and propagates the state of the system forward one time step.

The PVT data is supplied by the user as a table of gas volumes and viscosities as a function of pressure. The data need not be at equal pressure intervals. The initialization code generates the table of the real gas potential and other finely spaced tables of PVT data used by the PVT lookup subroutine in the time stepping calculation. The table lookup uses linear interpolation in an equally spaced table. The fracture network is represented to the simulator as a table that contains the coordinates of the fracture endpoints and the fracture apertures. The code determines the fracture intersections (nodes), assigns indices to the nodes, and then creates a set of indexing arrays that specifies the geometric relationship of the nodes with their neighboring nodes. The initialization code also calculates all the geometric coefficients (fracture transmissibilities and recharge model pore volumes and transmissibilities) required for calculation of flow rates in both the fracture network and the recharge models.

The fracture transmissibilities are calculated from the segment lengths, formation thickness, and fracture aperture using the cubic law for laminar flow between parallel plates. The pore volumes and transmissibilities for a recharge model are calculated from the effective volume and flow path length assigned to the model based on the geometric relationship of the bounding fracture segments. The effective volumes for the recharge models are divided into a number of blocks. The number of blocks ranges from one to the maximum number of blocks permitted by the code depending on the flow path length. The volumes with the longest flow paths are divided into the maximum number of blocks, and volumes with shorter flow paths are divided into correspondingly few blocks. The block lengths for a given volume are assigned geometrically. The shortest block is adjacent to the fracture face and the block lengths increase in size so that the block with the greatest length is most distant from the fracture face. Once the block lengths have been computed, the corresponding pore volumes and transmissibilities for the recharge models are calculated and stored.

The control and recurrent data interface is designed to provide flexible control of the wells and the graphical output. It permits the specification of individual well operation. The bottom hole pressure or gas flow rate is specified for each well independently and may be changed any number of times during the simulation. Graphic displays of well data and the reservoir pressure field may be scheduled according to the user needs. Each of the displays is independent of all others. The displays may be scheduled to occur only once or on a periodic basis, and the period may be changed at anytime during the simulation run.

The solution propagator section is the heart of the simulator and is based on conservation of mass. The computational sequence is as follows. The recharge models are called to update their rates of recharge to the fractures. Next, the material balances are calculated at all nodes and recharge points. If all balances are within a specified tolerance, the state of the reservoir at the end of the time step has been obtained. If the tolerance is not met, a Newton-Raphson procedure is performed. This includes the formation of the coefficient matrix for the set of linear equations, solution of the linear equations by the linear solver, and application of the corrections to the potentials at the nodes and recharge points. The recharge rates are then recalculated, and new material balance computations are performed. The procedure continues until all the material balances meet the specified tolerance. Once the solution has converged, the production history of each well is updated. Although the internal calculations are in terms of the potential, the code makes the conversion so that all input and output is in terms of pressure.

Now that the simulator has been described, we can address the modifications that are needed in order to use it for simulation of enhanced gas production/CO2 sequestration projects. The major modification is the expansion of the calculation from a single component to multiple components. There is also the need to modify the calculation of the gas stored in the rock matrix to include adsorbed gas as well as free pore gas. Although all three sections of the code require some modification, the most extensive and most difficult are those to the solution propagator section. The modification to the solution propagator consists of adding material balances for individual components to the overall mass balance. Because of the constraint that mole fractions must sum to one, we need to add one less equation than the total number of species. Although all the balances could be solved simultaneously, a more computationally efficient method is to solve the overall material balances first to obtain the potential distribution and then move the chemical species according to this potential distribution. Such a procedure is called a sequential method.

In the sequential method, the form of the equations for the overall material balances does not change from the single component case; however, the PVT properties of the gas become functions of composition as well as pressure. Thus, the potential becomes a function of composition. This necessitates the modification of the PVT lookup routines so that they interpolate on both pressure and composition. The component material balance equations that are solved once the potential distribution is obtained are linear algebraic equations. The only complicating factor is that use is made of the technique known as upstream weighting. Upstream weighting insures that the composition at a given node is dependent on the composition at nodes that are upstream in the flow path but unaffected by the composition at nodes that are downstream. The complexities that this introduces will be discussed in the implementation section of the report. The difference in structure of these equations requires a different linear solver, but the same successive over-relaxation method can still be used. No iteration is required.

The recharge models also require an added step that updates the compositions once the potential field has been obtained. The algebraic equations that need to be solved are obtained by discretizing the PDEs that describe the composition changes in space and time. The discretization method is the same as that used in the overall balance PDEs, except that upstream weighting is used. The equations are linear and can be solved without iteration if it is assumed that the adsorption isotherms may be linearized about an operating point. If this approximation is made, the inclusion of adsorption is easily included. These equations are also tridiagonal and are solved by the Thomas algorithm.

The implementation of the modifications to the recharge models and the PVT lookup were easily accomplished

and presented no difficulty. The addition of the component balances in the fracture network appeared at first to be a complex issue because of the upstream weighting. Initial analysis indicated that the equation set could be solved by eliminating the composition at the nodes and solving the set of equations for the compositions at the recharge points. This approach resulted in a complex set of couplings between the unknowns that made the generation of coefficients for the linear equations and the programming of the linear solver rather complex. A new indexing array was added to the simulator, and the code to generate the indices was added to the initialization section. During the process of integrating all the changes into the code, it was found that there was a much better way to solve these balance equations. Re-analysis showed that, by using a two-step process of looking at recharge points upstream of nodes and then looking at the nodes upstream of these recharge points, the composition at the recharge points can be eliminated from the set of equations. The resulting set of equations has a simple form. The coefficient matrix is easily generated and the linear solver easily programmed. Work on this part of the code was in progress at the end of FY01. Work on these changes should be completed during Jan. 2002.

Modeling Gas Hydrate Formation in Pores

The first objective of this work was to develop a model that will enable prediction of the formation pressure of gas hydrates in sediments. Due to the effects of capillary pressure, the conditions under which hydrates form in sediments can be very different from those in the bulk. A second objective was related to concerns about the potential effects of rising carbon dioxide levels in the atmosphere, which have stimulated interest in a number of carbon dioxide sequestration studies. One suggestion is to sequester carbon dioxide as clathrate hydrates by injection of carbon dioxide into methane hydrate. Energy supply research estimates indicate that natural gas hydrates in arctic and sub-seafloor formations contain more energy than all other fossil fuel deposits combined. The simultaneous sequestration of carbon dioxide and the production of methane by injection of carbon dioxide into deposits of natural gas hydrates, if possible, represent a potentially efficient and cost effective option for the sequestration of carbon dioxide. Data in the literature show that the conversion of bulk methane hydrate into carbon dioxide hydrate is thermodynamically favored. These results are not directly applicable to naturally occurring hydrates, because the hydrates in these locations are embedded in sediments. The thermodynamics of any potential conversion of CH_4 hydrate to CO_2 hydrate will therefore be affected by the size of the pores in which the conversion of CH_4 hydrate to CO_2 hydrate would take place. Therefore, it was necessary to develop a model capable of calculating the heats of formation of these hydrates in porous media as a function of pore size and temperature. Such calculations allow for an assessment of the thermodynamic feasibility of converting CH_4 hydrate to CO_2 hydrate in porous media involving various size pores.

A computer program has been developed which is capable of predicting hydrate formation in bulk hydrates, as well as in pores. The model is based on a statistical thermodynamic approach to predict the formation conditions for gas hydrates. In addition, a new conceptual model of hydrate decomposition in pores has been constructed to allow for the consideration of the effects of the distribution of pore sizes present in real porous media. The results of using this model to reconstruct the pore volume distribution of the porous medium were in good agreement with the distribution obtained from other methods, thus validating the model.

BIO-HYDROGEN PRODUCTION:

Achieving a continuous hydrogen production system requires an understanding of the biochemistry of

the process. Since beginning this project, we have determined the most important conditions for optimal hydrogen production by *Thermotoga neapolitana* and have tested all of the other available members of this order for their ability to produce hydrogen gas. We have found that *Thermotoga neapolitana*, *Thermotoga elfeii* and *Fervidobacterium pennavorans* are the most productive strains of bacteria tested. In batch experiments lasting less than a week, each of these strains has produced in excess of 30% hydrogen in the resultant gas mixture. Batch experiments are necessarily limited to less than a week because the pH rapidly decreases, and the oxygen is rapidly used up. We have discovered that salinity, temperature, and pH are very important variables. We have obtained most of the equipment needed for qualitative and quantitative on-line analysis of hydrogen gas production using continuously stirred tank reactors and ancillary analytical tools. Each of the components of this system have been tested and calibrated separately. The components will now be integrated as we begin shakedown of the entire continuous analysis system. Utilizing this system is expected to be an essential activity in FY02.

We have also discovered that low levels of oxygen are crucial for high hydrogen production. In the presence of 4-12% oxygen, hydrogen production is invariably high, and the oxygen levels decrease to less than 1% during the course of active hydrogen evolution. When oxygen levels are reduced to below 3%, hydrogen production is much reduced. This is a very surprising finding, since the literature suggests that the *Thermotogales* are obligate anaerobes. (Obligate anaerobes are organisms that die in the presence of <u>any</u> oxygen.)

The need to provide oxygen to the batch reactor system in order to obtain a high hydrogen output is a very exciting finding, and far from just a curiosity, because it suggests that perhaps the metabolic behavior of these cells is not fermentative, but that these bacteria may actually be respiring (using the available oxygen to assist in the complete breakdown of carbon feedstocks). Fermentative processes (which partially break down carbon feedstocks) have been estimated to be 20-30% efficient. By contrast, respiratory processes completely utilize carbon feedstocks and can be up to 100% efficient.

We believe our organisms are respiring rather than fermenting for the following reasons. Our results to date indicate that the efficiency of *Thermotoga neapolitana* for utilization of glucose as a carbon source is conservatively 50%--much too high to occur by classical fermentation. Furthermore, high hydrogen production only occurs when there is 4-12% oxygen in the headspace at the start of the experiment. We have also shown that malonate, a specific inhibitor of respiration, inhibits both growth and hydrogen production.

We are currently attempting to determine how the oxygen that these cells require is used. In part, we are using an ion chromatograph to analyze the used growth medium to determine if any substances not seen in the controls are seen in the medium where the bacteria have grown.

We are still awaiting acceptance of our first patent for this process. Our initial work suggests that it may be possible to use these organisms in an even greater number of ways to produce hydrogen. Our more recent findings will most likely necessitate filing a second patent application.

We are currently developing a rapid screening method for determining how wide a range of feedstocks each of the different genera and species in the order *Thermotogales* can metabolize. To do this, we are adapting an existing technology developed by Biolog that examines 95 different potential feedstocks per

trial. This process is currently working, and we are standardizing the results. We will use Biolog software to develop an identification database for the order *Thermotogales*. We are also considering possible development of a CRADA with Biolog to continue and expand this work.

Meanwhile, laboratory research continues and has three main goals:

1. Continue research to determine the mode of metabolism used by these organisms to break down (catabolize and use) carbon sources to provide energy.
2. Complete the assembly of a scale-up apparatus to go from laboratory- to bench-scale.
3. Screen all hydrogen producing species of the *Thermotogales* to determine how great a variety of carbon sources they can use, and in particular, which of them can grow on cellulose.

We are currently preparing to scale up our existing batch process so we can develop a continuous process for hydrogen generation. This will bring us one step closer to developing a commercial process for hydrogen production. The way we have chosen to organize this scale-up process will allow us to monitor on line the input gas (flow rate and composition), the output gas (flow rate and composition), pH, pCO_2, and cell density. In addition, we will be able to monitor the concentrations of glucose, lactate, acetate, ammonium, sodium, potassium, glutamine, and glutamate on line. To further assist in determining exactly how hydrogen is being produced and to maximize that production, we will utilize a Coulter counter to verify cell counts and an ion chromatograph to monitor the liquid for any unexpected products secreted by the bacteria into the growth medium.

Gas chromatographs are currently used to determine gas concentrations for our batch experiments. While adequate for batch experiments, gas chromatography can only assay grab samples. In addition, many questions cannot be answered with this technology. Thus, an essential feature of our scale-up system is the introduction of a mass spectrometer to measure gases. This system will be able to monitor gas evolution on-line. It is also able to detect stable isotopes of the various elements, so it will allow us to unambiguously answer such questions as: Are these organisms able to “fix” molecular nitrogen? Where does the molecular oxygen go when it is taken up from the headspace? Is there a difference in hydrogen production between those cells that are growing and those that are not? The answers to all of these questions are extremely important to development of a viable, sustainable commercial process for hydrogen production.

Bacteria are able to use a variety of carbon sources as food. The carbon sources used have been shown to be specific to the bacteria using them. Thus, we are developing a protocol to rapidly (1-3 days) screen bacterial utilization of 94 different carbon sources. While this technology is not new and has been largely developed by Biolog, it has never been adapted for use to screen thermophilic bacteria. We will examine 20 different strains of the order *Thermotogales* (each of them already known to produce hydrogen) to determine their carbon source preferences.

One essential result will be to determine which of these bacterial strains are capable of utilizing cellulose. Cellulose is a very abundant carbon source and is a chief component of wood and forest products as well as of the pulp and paper making industry. One long-term goal of this work is to develop a sustained commercial process for producing hydrogen fuel from organic waste, such as wood waste.

FY 2001 Publications and Presentations

Kal Seshadri, Joseph W. Wilder, and Duane H. Smith. Measurements of equilibrium pressures and temperatures for propane hydrate in silica gels with different pore size distributions. J. Phys. Chem. 105(13).

J. W. Wilder, K. Seshadri, and Duane H. Smith, Assessing the thermodynamic feasibility of the conversion of methane hydrate into carbon dioxide hydrate within porous media. Proc. First National Conf. Carbon Sequestration.

Joseph W. Wilder, Kal Seshadri, and Duane H. Smith. Modeling hydrate formation in media with broad pore size distributions. Langmuir.

Joseph W. Wilder, Kal Seshadri, and Duane H. Smith. Resolving apparent contradictions in equilibrium measurements for clathrate hydrates in porous media. J. Phys. Chem.

Duane H. Smith, Joseph W. Wilder, and Kal Seshadri. Methane hydrate equilibria in silica gels with broad pore size distributions. AIChEJ.

G. Ahmadi, M. Shams, and D.H. Smith. Flow and sediment deposition in meandering rivers. Appalachian Rivers III Conference, Proceedings.

Measurements of equilibrium pressures and temperatures for propane hydrate in silica gels with different pore-size distributions. J. Phys. Chem.

Modeling Hydrate Formation in Media with Broad Pore Size Distribution" and "Resolving Apparent Contradictions in Equilibrium Measurements in Clathrate Hydrates in Porous Media" have just been accepted for publication.

Bio-hydrogen production by the thermophilic bacterium *Thermotoga neapolitana*. Applied Biochemistry and Biotechnology.

The bio-hydrogen work was also presented orally and as posters at two national hydrogen meetings, and at the International Energy Agency Annex 15 Biohydrogen Meetings held in Porto, Portugal this spring, and the Joint COST/IEA International Meeting in Szeged, Hungary.

Thermotoga neapolitana: A microaerophile producing hydrogen in the presence of oxygen, has been accepted for presentation at the 5th Annual Biomass Conference of the Americas in Orlando, Florida.

Publications that have not yet been accepted:

Duane H. Smith, J. W. Wilder, and K. Seshadri. Thermodynamics of sequestration of carbon dioxide in natural gas hydrates in porous media: complete conversion of methane/propane hydrates into carbon dioxide hydrate. Proc. ECCS/IEA Meeting, submitted.

Joseph W. Wilder and Duane H. Smith. Dependencies of clathrate hydrate dissociation pressures on the inverse temperature and inverse pore radius. J. Chem. Thermo., submitted.

Joseph W. Wilder and Duane H. Smith. Upper limits on the rates of dissociation of clathrate hydrates. Ind. Eng. Chem. Res., submitted.

Joseph W. Wilder and Duane H. Smith. Comments on "Aanomolous preservation of pure methane hydrate at 1 atm.". J. Phys. Chem. B, submitted.

Kal Seshadri, Joseph W. Wilder, and Duane H. Smith. Thermodynamics of hydrogen sulfide clathrate

hydrate in porous media. In preparation.

Wu Zhang, Joseph W. Wilder, Kal Seshadri, and Duane H. Smith. Equilibrium pressures and temperatures for ethane hydrate in silica gels with different pore size distributions: Evidence for a model for the phase equilibria of hydrates in porous media. Langmuir, in preparation.

Kal Seshadri, Joseph W. Wilder, and Duane H. Smith. Thermodynamics of carbon dioxide hydrate formation in porous media. In preparation.

Duane H. Smith, Kal Seshadri, Wu Zhang, and Joseph W. Wilder. Heats of dissociation of some clathrate hydrates in porous media. In preparation.

G. Ahmadi and D.H. Smith. Analysis of backpulse process for a hot-gas filter vessel. Aerosol Science and Technology, in press.

G. Ahmadi and D.H. Smith. Gas flow and particle deposition in the hot-gas filter vessel of the Pinõn Pine Project. Powder Technology, submitted.

References

Angus, S., Armstrong, B., & de Reuck, K. (1976). International Thermodynamic Tables of the Fluid State, Carbon Dioxide. Oxford: IUPAC, Pergamon Press.

Angus, S., Armstrong, B., & de Reuck, K. (1978). International Thermodynamic Tables of the Fluid State - 5 Methane. Oxford: IUPAC, Pergamon Press.

Bakker, K. (1997). Using the finite element method to compute the influence of complex porosity and inclusion structures on the thermal and electrical conductivity. Int. J. Heat Mass Transfer, 40(15), 3503-3511.

Buonanno, G. & Carotenuto, A. (1997). The effective thermal conductivity of a porous medium with interconnected particles. Int. J. Heat Mass Transfer, 40(2), 393-405.

Collett, T. (1995). Gas hydrate resources of the United States. National Assessment of United States Oil and Gas Resources – Results, Methodology, and Supporting Data, Gautier, D. et al., (Eds.), U.S. Geological Survey Digital Data Series 30.

Douslin, D. & Harrison, R. (1973). Pressure, volume, temperature relations of ethane. J. Chem. Therm., 5, 491-512.

Eubank, P. (1972). Thermodynamic properties of ethane: Vapor-liquid coexistence. Advan. Cryog. Eng., 17, 270-281.

Feder, J. (1988). Fractals. New York: Plenum Press.

Ferer, M., Bromhal, G., & Smith, D. (submitted 2001). Pore Level Modeling of immiscible drainage. Groundwater.

Ferer, M., Sams, W. N., Geisbrecht, R. A. & Smith, D. H. (1991). Scaling of Fractal Flow, Physica A **177**, 273-80.

Ferer, M., Geisbrecht, R. A., Sams, W. N. & Smith, D. H. (1992). Cross-Over from Fractal to Compact Growth in Simulations of Two-Phase Flow with Finite Viscosity Ratio in Two-Dimensional Porous Media, Phys. Rev. **A 45**, R6973-76.

Ferer, M., Geisbrecht, R. A., Sams, W. N. & Smith, D. H. (1993). The Fractal Nature of Viscous Fingering: Saturation Profiles and Fractional Flows from Modeling of Miscible Flow in Two-Dimensional Pore Level Models, in Proc. SPE Symp. Reservoir Simulation, New Orleans, Feb. 28-March-3, 1993, SPE 25270.

Ferer, M., Sams, W. N. Geisbrecht, R. A. & Smith, D. H. (1993). Crossover from Fractal to Compact Flow from Simulations of Two-Phase Flow with Finite Viscosity Ratio in Two-Dimensional Porous Media," *Phys. Rev. E* 47, 2713-23

Ferer, M. & Smith, D. (1994). Interfacial width. Phys. Rev. E, 49, 4114.

Ferer, M., Sams, W. N., Geisbrecht, R. A. & Smith, D. H. (1995). The Fractal Nature of Viscous Fingering in Two-Dimensional Pore Level Models," AIChEJ, 41, 749-63

Ferer, M., Gump, J. & Smith, D. (1996). 3d fractal crossover. Phys. Rev. E, 53, 2502-2508.

Handa, Y. & Stupin, D. (1992). Thermodynamic properties and dissociation characteristics of methane and propane hydrates in 70-Å-radius silica gel pores. Journal of Physical Chemistry, 96, 8599-8603.

Holder, G., Zetts, S., & Pradhan, N. (1988). Phase behavior in systems containing clathrate hydratres: a review. Review in Chemical Engineering, 5(1-4), 1-70.

Jannesh, H., Huber, R., Belkin, S., & Stetter, K. (1988). *Thermotoga neapolitana* sp. nov. of the extremely thermophilic, eubacterial genus *Thermotoga.* Arch. Microbiol. 150,103-104.

Koch, R., Canganella, F., Hippe, H., Jahnke, K. & Antranikian, G. (1997). Purification and properties of a thermostable pulluanase from an newly isolated thermophilic bacterium, *Fervidobacterium pennavorans* Ven5. App. Env. Microbiol., 63(3), 1088-1094.

Kono, H.O., Narasimhan,S., Song,F.& Smith, D.H. (2001). Synthesis of methane gas hydrate in porous sediments and its dissociation by depressurization. Powder Technology.

Makogon, Y. (1997). Hydrates of Hydrocarbons. Tulsa, OK: PennWell Books.

Meakin, P. (1998). Fractals, scaling, and growth far from equilibrium. Cambridge: Cambridge University Press.

Misra, A., Becker, R. & Fricke, B. (1995). A theoretical model of the thermal conductivity of idealized soil. HVAC&R Research, 1(1), 81-96.

Ravot, G., Magot, M., Fardeau, M., Patel, B., Prensier, G., Egan, A., Garcia, J. & Ollivier, B. (1995). *Thermotoga elfeii* sp. nov., a novel thermophilic bacterium from an African oil-producing well. J. Syst. Bacteriol., 45, 308-314.

Singh, D. & Konchenapalli, D. (2000). Generalized relationships for estimating soil resistivity. Experimental Thermal and Fluid Science, 22, 133-143.

Sloan, E. & Dendy, Jr. (1998). Clathrate Hydrates of Natural Gases (2nd. ed.). New York: Marcel Decker.

Smith, D., Covatch, G., & Lawry, Jr., W. (1992). Three-fluid wetting transitions and their effects on three-phase flow through porous media. SPE Formation Evaluation, 323-330.

Stern, L., Kirby, S., & Durham, W. (1998). Polycrystalline methane hydrate: synthesis from superheated ice, and low-temperature mechanical properties. Energy & Fuels, 12, 201-211.

Sychev, V. et al. (1987). Thermodynamic Properties of Ethane. New York: Hemisphere Pub. Co. (Harper & Row).

Thauer, R., Jungerman, K., & Decker, K. (1977). Energy conservation in chemotropic anaerobic bacteria. Bacteriol. Rev.41, 100-180.

Tulk, C., Ripmeester, J., & Klug, D. (1992). The application of Raman spectroscopy to the study of gas hydrates. Annals of the New York Academy of Sciences, 912, 859-872.

Van der Waals, J. & Platteeuw, J. (1959). Adv. Chem. Phys., 2, 1-57.

Vicsek, T. (1989). Fractal Growth Phenomena. Singapore: World Scientific.

Zhang, W. & Smith, D. (submitted). Conflict and solution in constructing thermodynamic equations for different integration paths. 4th International Conference on Natural Gas Hydrates.

Zhang, W., Wilder, J., & Smith, D. (submitted). Equilibrium pressures and temperatures for ethane hydrate in silica gels with different pore-size distributions: Evidence for the hydrate--water interface model for phase equilibria of hydrates in porous media. Langmiur.